DEVELOPMENT AND VIABILITY OF AN INVERTED DESCENT QUADROTOR

FOR PRECISION AERIAL DELIVERY

A Thesis
IN
Mechanical Engineering

Presented to the Faculty of the University
of Missouri–Kansas City in partial fulfillment of
the requirements for the degree

MASTER OF SCIENCE

by
SEAN WARD

B. S., University of Missouri - Kansas City, 2020

Kansas City, Missouri
2021

DEVELOPMENT AND VIABILITY OF AN INVERTED DESCENT QUADROTOR FOR PRECISION AERIAL DELIVERY

Sean Ward, Candidate for the Master of Science Degree

University of Missouri–Kansas City, 2021

ABSTRACT

The field of Precision Aerial Delivery strives for the highest standard of accuracy, with sights set on delivering payloads from high altitudes to mere feet from goal locations. Quadrotors, due to high maneuverability and precision, are a logical choice to achieve this objective, however current inefficiencies of descent prevent quadrotors from use in Precision Aerial Delivery.

Described herein are the development, experimentation and implementation of a near passive, Inverted Descent Quadrotor system. The Inverted Descent Quadrotor allows for high altitude deployment of a quadrotor fitted with standard hardware with the ability to descend more rapidly and with less energy requirement than previously possible. The decreased energy requirement of the Inverted Descent Quadrotor enables quadrotors to be used in high altitude scenarios, for missions that have previously been reserved for guided parachute or parafoil systems. Quadrotor systems thrive in such missions after descent,

as they accommodate the potential for complex, highly precise activities to be completed once reaching ground.

The development process consisted of wind tunnel thrust testing, a proof of concept single axis prototype, a functional Inverted Descent Quadrotor build, real world performance testing and mission simulation. Each stage of development provided valuable insight into the governing dynamics of rapid descent environments and informed the subsequent phases of development.

Wind tunnel thrust testing helped to identify a potentially optimal baseline throttle to apply when facing high speed descent to maintain control authority, as well as quantify potential power savings. The single axis prototype proved control potential in an artificial descent environment, further quantified power usage, characterized potential glide performance and suggested control gains for the rapid descent environment. A functional Inverted Descent Quadrotor was then built and tested to prove initial functionality, and verify the results from single axis testing. The system was then tested to quantify control, power and glide performance against various configurations of normal quadrotor descent, as well as current comparable Precision Aerial Delivery Systems. Finally, the Inverted Descent Quadrotor′s performance results were extrapolated to simulation to display the increased performance of the Inverted Descent Quadrotor in a mission setting.

The Inverted Descent Quadrotor proved to be successful in reducing descent energy, which endowed high precision quadrotor systems the capability for descents far

higher than previously possible. With far less sensitivity to wind prediction, coupled with the potential for payload capacity, the Inverted Descent Quadrotor showed promise worthy of future development and research.

APPROVAL PAGE

The faculty listed below, appointed by the Dean of the School of Computing and Engineering, have examined a thesis titled "Development and Viability of an Inverted Descent Quadrotor for Precision Aerial Delivery," presented by Sean Ward, candidate for the Master of Science degree, and hereby certify that in their opinion it is worthy of acceptance.

Supervisory Committee

Travis Fields, Ph.D., Committee Chair
Department of Civil & Mechanical Engineering

Mujahid Abdulrahim, Ph.D.
Department of Civil & Mechanical Engineering

Gregory King, Ph.D.
Department of Civil & Mechanical Engineering

CONTENTS

ILLUSTRATIONS

TABLES

ACKNOWLEDGEMENTS

I would like to thank my academic advisor, Travis Fields for all of his guidance as well as the opportunity to be a part of the Parachute and Aerial Vehicle Systems Lab. I would also like to thank Dr. Abdulrahim and Dr. King for participation in my graduate committee.

A special thanks to everyone in the PAVS Lab at UMKC including Paul Klappa, Cody Smith,, Simeon Karnes, Jackson Daniel, Shawn Herrington and others. And of course, a big thank you to Justin Nguyen for all the help. I would also like to thank my family for making this possible.

CHAPTER 1

OVERVIEW

1.1 Motivation

Specifically in military operations, there are a wide variety of situations that require the precision delivery of payloads. Resupply through precision guided airdrop systems can be invaluable to military operations, providing ground support with everything from ″a pin-point delivery of medical supplies, sensors, [to] ground robots″ [1]. While in many cases these payloads require high precision and rapid delivery, missions often require the deployment of the systems from relatively high altitudes due to safety concerns if in hostile territory. Methods of precision aerial delivery (PAD) have improved remarkably in recent years, however, nearly all PAD systems to date rely on a parachute/parafoil as the primary method of descent. While relatively effective for larger payloads, such systems are plagued by slow descent speeds and relative lack of precision for small, high consequence delivery.

With recent improvement in quadrotor control systems, quads have become a viable alternative in small payload delivery. Quadrotors could alter the landscape of potential missions, as they can complete complex, high precision movements, making them preferable in certain scenarios to their parachute/parafoil counterparts. For instance, quadrotors would be invaluable in urban operations, which are expected to be ″an unavoidable aspect of future military operations″ despite the fact that upon assessment, ″the

US military, as currently structured, is grossly unprepared for″ such operations [2]. Or in the case of reconnaissance, rather than a ground robot carried by a PAD system, use of a quadrotor simplifies a potentially complex mission, by acting as both the delivery system as well as the reconnaissance vehicle.

Issues arise, however, when attempting to integrate quadrotor delivery systems into high altitude environments. Quadrotors depend on all motors to maintain control, requiring that all motors are powered during descent. High altitude deployment of quadrotors results in a decrease in control effectiveness and increase in power requirement due to lower air density, but more importantly a slower than ideal descent velocity due to a phenomenon called the Vortex Ring State (VRS).

Vortex Ring State occurs due to the quadrotor descending into the turbulent downwash from its propellers, resulting in loss of control and oftentimes crashes. The VRS severely limits descent maneuverability due to induced instability during high speed descents [3]. This hinders the use of quadrotor systems for high altitude precision payload delivery, as the quadrotors require too much energy for descent to make the system feasible.

This body of work examines the application of an Inverted Descent Quadrotor, in which a quad would be deployed upside down, descending at near terminal velocity while the air from descent spins the rotors in their correct directions, allowing for control during the descent. Inverted descent is a promising method of descent that would eliminate the loss of control, high power requirement, and slow descent speed that plague normal quad descent systems and overcome the lack of precision and slow descent speeds that

parachute/parafoil PAD systems face.

1.2 Objectives

The Inverted Descent Quadrotor consists simply of a standard fixed prop quadrotor utilizing custom control firmware and control gains, deployed upside down for the duration of its descent. Once reaching a sufficiently low altitude, the quad performs a half flip, righting itself and allowing for normal quadrotor function to resume. In theory, the system would be able to descend far faster than normal quadrotor descent, while maintaining sufficient attitude control and minimizing power requirement.

The goals of this thesis were to thoroughly explore the viability of inverted descent, which followed a process described in Figure 1. After initial screening experiments to validate the viability of the system, a major part of this process was first to successfully design and implement the system into a quadrotor. Then experiments and real world testing could be performed to acquire data on the performance of the system and how it compares to current alternatives. Finally, the performance metrics acquired from the testing and experiments could be extrapolated in simulation to identify the relative strengths and weaknesses of the system.

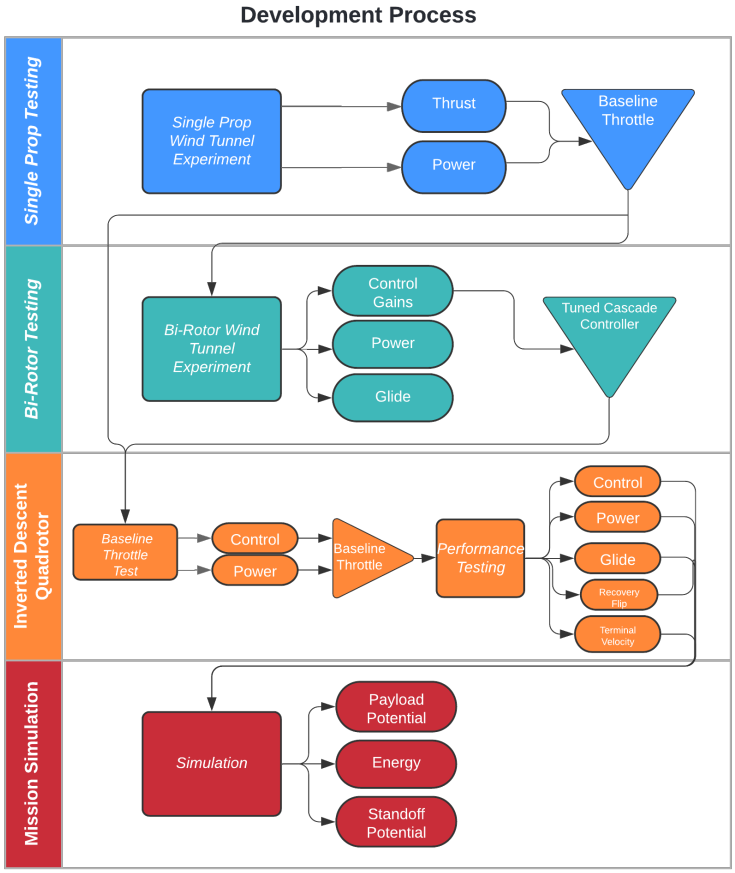

Figure 1: Development Process

The main contributions of this work are as follows:

- The potential of Inverted Descent is tested and quantified in wind tunnel environment
- The performance of an Inverted Descent Quadrotor is quantified and compared to normal descent
- Methods are simulated in mission environments for comparison with current industry Precision Aerial Delivery systems

Chapter 1 described the motivation, objectives and contributions of the work as a whole. Provided in Chapter 2 are the background and relevant literature necessary to provide further context to the work. Chapter 3 describes and summarizes the preliminary wind tunnel testing and initial single axis prototype experiment performed to help quantify the potential of inverted descent.

Chapter 4 outlines the fully functional Inverted Descent Quadrotor build, and testing conducted in efforts to identify a potentially optimum baseline throttle. Testing is expanded on in Chapter 5, which details the full factorial descent experiment performed with intention of quantifying both normal and inverted quadrotor descent. The performance characterized in Chapter 5 was then extrapolated to mission scenarios in Chapter 6, providing a more realistic comparison of the Inverted Descent Quadrotor developed to current PAD methods. Finally, the results of the work as the whole are summarized in Chapter 7, along with areas for future work and development.

CHAPTER 2

BACKGROUND AND LITERATURE REVIEW

2.1 Precision Aerial Delivery

While aerial delivery systems have been used in military and civilian applications since as early as the 1940s, recent developments in computing and trajectory planning have made precision aerial delivery possible from increasing altitudes with increasing precision. The U.S. military quickly capitalized on these advances, developing the Joint Precision Aerial Delivery (JPAD) program in 1998 [4]. Essentially, the JPAD program implemented cutting edge autonomous guidance units (AGUs) integrated into payloads, which could then assimilate weather information from various sources and build trajectories to improve delivery accuracy [5].

In short, JPAD allowed for more flexible delivery systems, unconstrained to detection or threat seen in theater level supply chains such as land resupply. This newfound flexibility allowed for multiple entry points, changes of delivery points enroute, and the ability to circumvent remote and compartmentalized terrain [6]. However, these benefits do not come without drawbacks, as these precision systems require expensive autonomous guidance units (AGUs), are plagued by relatively slow descent speeds and still hold a degree of inaccuracy in point of impact.

The relevant class of PAD systems which quadrotor systems would potentially fall into is the lower end of the ultra-light/micro light class, corresponding to payloads from

1 to 50 lbs. This class of systems are utilized in delivering low weight, high consequence items such as therapeutics, medical equipment, combat care kits, combat critical care systems, expendable resupply items for biological detection systems, prophylaxis, and robot/sensor/psyop systems [7].

There are several predominant PAD systems in this weight class that are used in industry as seen in Table 1, each using a precision guided parachute/parafoil based approach. The precision/accuracy of these methods is most commonly quantified using the Circular Error Probable (CEP), describing radius of circle centered about the intended impact point statistically likely to contain 50% of the impact points [8].

Table 1: Comparison of Current PAD Systems

System	Payload (lbs)	Glide	CEP (ft)
Mosquito	3 – 50	3	98
Micro Onyx	0 – 20	4	246
Snowflake ADS	0 – 3	2	82

While the majority of PAD systems in the ultra/micro light weight class are parauchute/parafoil based, the potential of quadrotor systems have not gone unnoticed. Increasingly complex systems have been implemented in an attempt to take advantage of the benefits of high precision quadrotor flight while overcoming the hurdles associated with quadrotor descent. One such system was the Autonomous Drone Delivery from Airdrop Systems (ADDAS) developed for the Natick Soldier Research Development and Engineering Center.

The ADDAS consists of a traditional autonomously guided parafoil system carrying sealed quadrotors, which descends from deployment altitude to $\sim$1000 ft AGL.

At this point, the quadrotor would be deployed via dispenser to complete the rest of the descent and mission. The system successfully demonstrated the potential to deliver payloads to within 16 feet of target coordinates at distances over 1/2 mile from release point [9]. The deficiencies of the ADDAS lie in the extensive measures necessary to eliminate prolonged quadrotor descent, which result in a complex system with many moving parts and consequently, potential failures. To achieve the greater precision and flexibility over more conventional systems, the ADDAS requires a precision guided parafoil system, a dispenser, as well as autonomous quadrotors.

The ADDAS project helped to highlight the fact that potential exists for immense improvements in accuracy through successfully implementing a quadrotor system into Precision Aerial Delivery. Quadrotors could facilitate an age abundant with novel mission possibilities, previously impractical for parachute/parafoil delivery methods. The inefficiency issues plaguing quadrotor descent hinder this evolution though, and necessitate the convoluted methods for quadrotor use seen in the ADDAS. The challenges faced by quadrotor PAD systems arise in large part due to a phenomena known as the Vortex Ring State (VRS).

2.2 Vortex Ring State

The VRS has been extensively researched in the context of helicopters, with recent exploration in quadrotor systems. The driving principle behind VRS is the fluctuations in rotor thrust, due to descent into its own turbulent rotor wash. These fluctuations in thrust manifest as nonlinearities, which result in instability that can lead to complete losses in

control and crashes [10].

VRS can be avoided by slowing the descent rate, or through generating a horizontal velocity component to translate outwards from the turbulent rotor wash. While quadrotors level of control and precision, coupled with high level of navigation autonomy makes them ideal for small payload delivery, the challenges associated with VRS make them impractical for high altitude deployment. High altitude deployment of a quadrotor followed by descent rates slow enough to avoid VRS would require substantial energy use in the descent phase, resulting in complete loss of battery before reaching ground.

General rules of thumb have been developed from lab testing, providing a definition of VRS through empirical data as shown in Figure 2b [10] coupled with analytical solutions in the form of the Oneras criterion from Figure 2a [10].

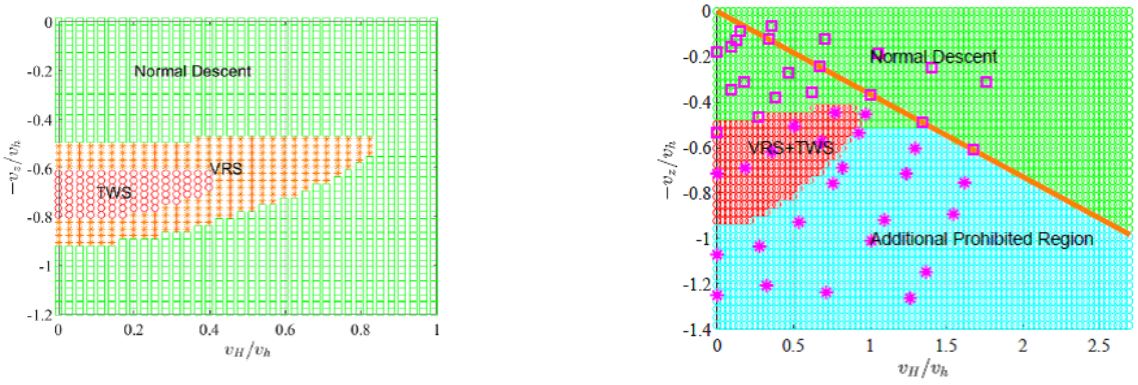

(a) VRS Analytical Identification

(b) VRS Experimental Identification

Figure 2: Analytical and Experimental VRS Identification

Using these guidelines, the horizontal velocity required to avoid VRS for any vertical descent velocity can be calculated using the weight of quadrotor, prop area, and

density of air as described in Equations 2.1 – 2.3 [10].

$$V_h = \sqrt{T_{hover}/2\rho A} \tag{2.1}$$

$$V_z \leq 0.5 V_h \tag{2.2}$$

$$V_H \geq \frac{V_z}{\tan 20^\circ} \tag{2.3}$$

Past research has shown that optimal paths can be developed to minimize time to descend, which does not correspond to shortest path to ground due to VRS challenges. The optimal path, shown in Figure 3 [10], is often a zig zag pattern comprised of oblique and flip maneuvers (if feasible), or corkscrewing descent patterns.

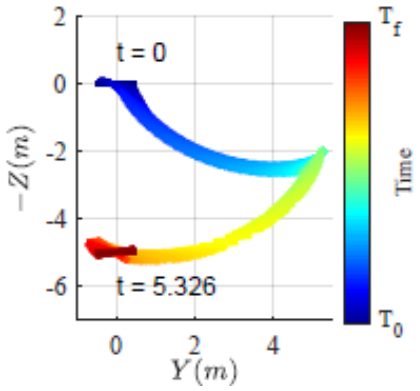

Figure 3: VRS Optimal Trajectories

The field of near passive descent looks to minimize the quadrotor energy squandered in descent, which would ideally liberate quadrotors from energy issues barring their use in PAD. Mitigating the energy required for descent would allow for quadrotor PAD

systems that could achieve unprecedented levels of accuracy and maneuverability without requiring complex systems to eliminate the descent phase altogether.

2.3 Near Passive Descent Methods

Near passive descent is a gold standard for quadrotor payload systems, as successfully developing a low power, controllable quad descent system would allow for complex and precise missions to be completed after deploying the quad from high altitudes. With the goal to minimize descent power requirement while maintaining control, to date several different methods of near passive descent have been explored for potential viability in work from Tiemann, as summarized in Table 2 [11]. Methods ranging widely from variable pitch quadrotors, reverse thrust quads, and inverted descent quads were vetted and tested to determine potential viability and performance.

While variable pitch quadrotors have shown promise in diminishing power requirement as well as maintaining control in descent, the complexity of the hardware posed vibration and structural challenges. Vibration issues resulted in the need to limit angular velocity, meaning the method had less thrust available. This reduced thrust potential resulted in the variable pitch quad struggling to support its own weight, much less have adequate headroom for a payload [11].

A reversible thrust system, utilizing reversible ESCs to change the direction of the motors would theoretically allow for effective control in a fast descent from altitude along with minimal power requirement. However, testing of this method proved ineffective, resulting in marginal control and comparable power consumption to normal descent [11].

Cost also proved to be a barrier, as reversible ESCs are far more expensive than their ordinary counterparts.

While the inverted method of near passive descent was not extensively field tested, the method showed promise in controllability as well as the potential for power savings. An additional benefit of this system lies in its simplicity. Making use of conventional quadrotor parts, such as fixed pitch props and one directional ESCs, would allow the system to not sacrifice carrying capacity, which would be vital for the system to be applied in payload delivery. With the right software changes to the controller, any quad could be adapted to utilizing this method of descent with off the shelf parts. For these reasons, summarized in Table 2 [11], the inverted system was deemed to have the highest potential and chosen for deeper exploration.

Table 2: Pugh Chart Comparison of Descent Methods

Criteria	Standard Quadrotor	Variable-Pitch	Reverse Thrust	Inverted Descent
Power Consumption	0	1	0	1
Control	0	1	0	-1
Mechanical Complexity	0	-1	0	1
Manufacturability	0	-1	0	0
Robustness	0	-1	0	0
Payload Capacity	0	1	-1	0
Standoff Distance	0	1	1	1
Descent Capability	0	1	1	1
Total	0	2	1	3

Other research [12] has investigated overcoming the challenges associated with VRS in quadrotors. The Yaw Rate Control method implemented a yaw rate during descent to maintain consistent thrust from propellers, which offset the need for horizontal velocity and the associated horizontal space to avoid VRS. The method displayed simplicity similar to inverted descent, requiring only standard hardware with control stack changes. However, while the method proved capable of increasing the descent velocity up to 3x while still avoiding VRS, power and energy was not discussed which would be vital to high altitude deployment. Even with 3x increases in descent rates, inverted descent showed more promise with expected descent rates of near terminal velocity. While promising, further exploration of this method would be necessary to determine the scalability and viability in high altitude PAD.

2.4 Dynamics of Inverted Flight

To control quadrotor attitude in an inverted regime, it is necessary to identify and note the differences from normal flight. The dynamics and associated control of normal quadrotor flight has been deeply explored in works such as [12], but little to no research has explored how these dynamics translate to the environment of inverted descent.

In normal quadrotor flight, motor thrust differentials provide control. For example, in the quadrotor cross configuration shown in Figure 4 [13], to achieve a positive roll angle (Right wing down) requires Motor 2 to spin slower and Motor 4 to spin faster, resulting in a net moment about the x axis. In the same way, to achieve a positive pitch angle (nose up) Motor 3 would spin slower and Motor 1 faster, to induce a pitching moment. Yaw angle is

controlled utilizing the induced drag from each propeller. Motors 1 and 3 spinning faster result in a counterclockwise body yaw moment, and Motors 2 and 4 spinning faster result in a clockwise body yaw moment.

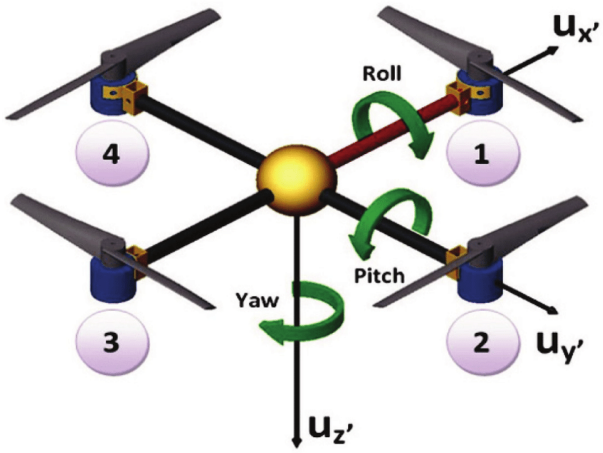

Figure 4: Normal Quadrotor Control

When inverted both the motor thrust vectors, as well as the polit frame control directions reverse. An increased thrust from any motor drives that motor downwards, rather than upwards in normal flight. As the quadcopter is flipped relative to the pilot, the yaw control motors are flipped from the normal case. Motors 3 and 4 spinning faster now results in a clockwise body yaw moment, and Motors 1 and 2 spinning faster now results in a counterclockwise body yaw moment. Roll and pitch control maintains the same control direction, meaning the same motor differential results in the same resulting moments in the body frame. However, in the most common method of attitude estimation, fusing accelerometer measurements with gyro readings, the inverted case flips the signs of roll and pitch angle estimation.

From the pilot frame, the flip axis affects the control directions of the roll and pitch axes. If the flip was initiated about the roll axis, Motors 2 and 4 have switched location relative to the pilot. This swap offsets the reversed attitude estimation in the body frame of the quadrotor, resulting in nominal control consistent with a normal flight controller with no change to motor actuation. The pitch axis on the other hand, suffers from the reversed attitude estimation, without the swapping of motor positions. Thus, the pitch gains must be flipped in sign to maintain consistent control from the pilot frame.

With rapid winds associated with inverted descent, even with no throttle the propellers would spin rapidly. The concept of baseline throttle was expected to be necessary to maintain control authority, by speeding the propeller slightly faster than that seen from the induced wind from descent to allow for larger thrust differentials both above and below the throttle trim condition.

The ability to translate and achieve useful movement to fight winds or track a desired trajectory during descent, was expected to result from the drag induced from the rapid descent as seen in Figure 5. The thrust component would fight this translational movement to a degree, as seen in Equation 2.4. The practical meaning being that increased baseline throttle was expected to provide increased attitude control, at the cost of both power and translational potential.

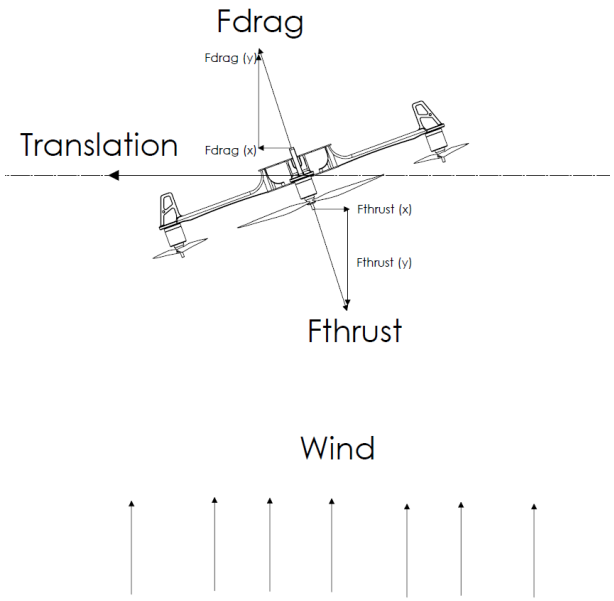

Figure 5: Free Body Diagram of Inverted Descent

$$\sum F_x = ma_x = F_{drag,x} - F_{thrust,x} \tag{2.4}$$

CHAPTER 3

WIND TUNNEL TESTING

In an attempt to further explore the viability of inverted descent, the case was first simplified to a single motor and propeller tested in a wind tunnel. The single propeller experiment was designed to prove whether or not control authority was even achievable at terminal wind speeds and if substantial power savings existed. A further goal was to quantify a suitable ″baseline throttle″ to apply to the system to maximize control authority with minimal power requirement.

After initially screening the potential benefits and feasibility of the inverted descent system through the single propeller testing, the testing process moved forward to testing a single axis, bi-rotor setup in the wind tunnel.

Two primary goals of the bi–rotor experiment were to validate the ideal baseline throttle identified in the single prop testing phase, as well as verify the potential control/power benefits of the inverted descent system as a whole. A further goal included performing gain tuning on the inverted system, as the differences from the normal regime of flight seemed sufficient that normal gain tuning would not be acceptable. The final goal of the bi–rotor setup was to identify glide characteristics that could be expected from the inverted system, as these would be crucial to the performance of the system in fighting winds and tracking positions during descent.

3.1 Single Propeller Testing

3.1.1 Methods

3.1.1.1 Physical Setup

All wind tunnel testing was performed using the FLOTEK 14400–90, while the configuration of the tunnel was changed to fit the required article into the wind stream. The FLOTEK 1440 boasts a 132 feet/sec maximum air velocity through its 12″ x 12″ x 36″ test section.

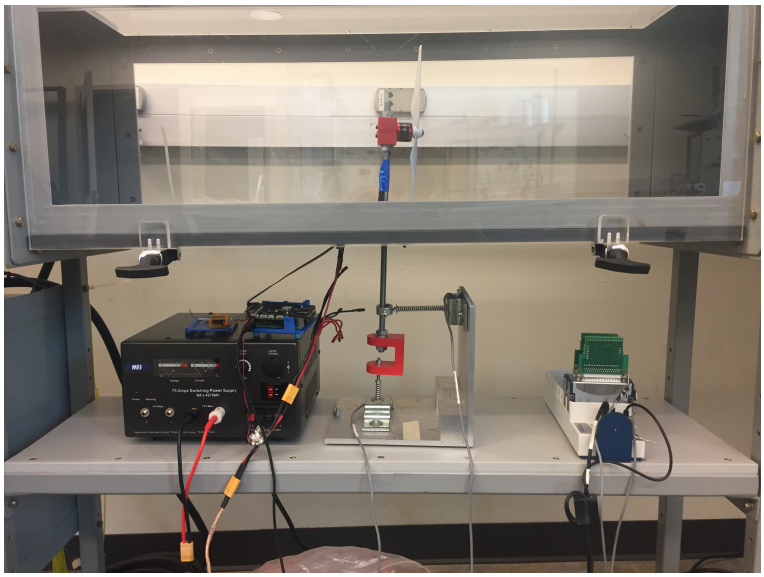

Figure 6: Single Propeller Wind Tunnel Test Setup

Accurate drag and thrust data was acquired using a load cell, connected to a DAQ system interfacing with LabVIEW. Custom 3d printed mounts were used to connect the single motor, prop, and accompanying ESC to the load cell stationed below the test section. The motor was powered though a power supply and received motor commands

from a Raspberry Pi 3 fitted with a Navio2 Autopilot hat, which served to also log both commands and current draw. Motor commands came from a Spektrum RC transmitter/receiver pair connected to the Raspberry Pi. The full single prop test setup can be seen in Figure 6.

3.1.1.2 Test Procedure

Testing was performed by changing air speeds from 37 – 95 ft/sec in 7 ft/sec increments. At each airspeed, the throttle for the motor was brought up from 0 – 100% in 11% increments, yielding 99 individual data points for comparison. Once steady state was reached for each configuration drag force and power consumption were logged for comparison. A control arm was also performed for comparison with no wind and throttle for this airspeed was changed in 10% increments due to post processing challenges.

The results were contextualized to the real world application of inverted descent, in which the vehicle would be judged on control at the cost of power requirement. Control was described by the ability to change the drag/thrust vector, allowing the quadrotor to maintain control of attitude. The derivative of drag/thrust with respect to throttle as described in Equation 3.1, helped quantify the potential control of each configuration.

$$ {}^{dDrag}/_{dThrottle} = \frac{\Delta Drag}{\Delta Throttle} \tag{3.1} $$

As increased control was expected to require increased power due to the increased baseline throttle, the cost of power was important to factor into the analysis. In an effort to find the potentially optimal region to yield highest level of control per power requirement,

the derivative of drag with respect to throttle (Eqn. 3.1) was then divided by the cost of power, calculated through Equation 3.2. This metric, dubbed ″Invert Ratio″ and shown in Equation 3.3, captured the potential of diminishing returns when increasing control.

$$Power(P_{inst}) = Vi \tag{3.2}$$

$$InvertRatio = \frac{{}^{dDrag}/_{dThrottle}}{Power} \tag{3.3}$$

3.1.2 Results

The relevant results from the single prop wind tunnel testing fell into two categories, power and potential for control. Testing yielded important insights to the potential viability of the inverted descent vehicle with regard to first whether it was possible, and then whether it would successfully provide substantial energy savings.

The likely region of operation of the inverted descent system was assumed to be from 0 ft/s, when the system initially started its descent, to roughly 88 ft/s which was estimated to be terminal velocity for the planned quadrotor. This region was analyzed to find a potentially optimum baseline throttle, allowing for the greatest control while minimizing power consumption.

As hypothesized, testing showed that increasing wind speeds at the same throttle command resulted in decreasing power draw on the system, as seen in Figure 7c. When compared to the no wind case, it was clear the potential for decreased power requirement existed. This verified one of the core theoretical principles driving the inverted descent,

that increasing winds resulted in less load on the motor.

Another interesting result from the testing was honing in on the location of force reversal for the prop, when it began generating thrust that was dominant over the propeller drag. At low wind speeds this occurred as early as 40% throttle, and above 59 ft/s it never occurred. This phenomena challenged another important theoretical assumption made in the conceptual phase of design, that drag would be the driving force for translational motion over propeller thrust. While the results suggested differently at wind speeds below 66 feet/sec with high throttle levels, it was important to remember that the setup had none of the drag associated with the frame that would be required in the final inverted system. The system drag was expected to increase significantly, which would situate drag as the dominant translational force of the system.

The loss of potential control authority at higher velocities was clear in Figure 7b, as higher wind velocity trended towards less ability to change drag. When comparing the wind configurations as a whole to the no wind case, it seemed there was potential for control authority relatively on par with normal flight, albeit decreasing with increasing descent speeds. While this lack of authority had potential to be overcome through increased baseline throttle, as seen in the peaks of each curve in the 70% – 90% range, it was unclear if the increased power associated with these higher throttles would be worth the increased control authority, or even necessary.

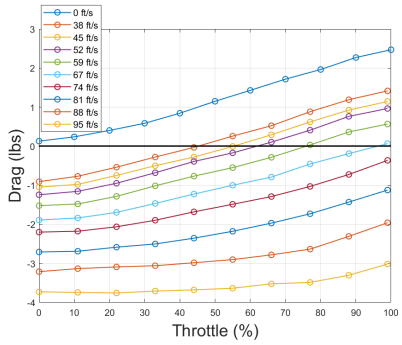

(a) Drag Force vs. Throttle Results

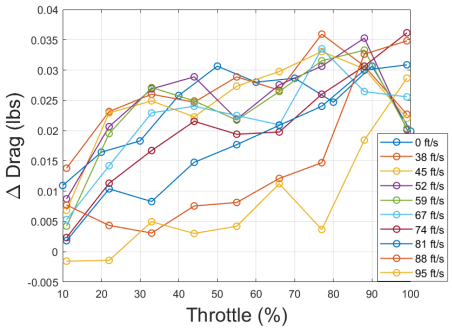

(b) dD/dt vs. Throttle Results

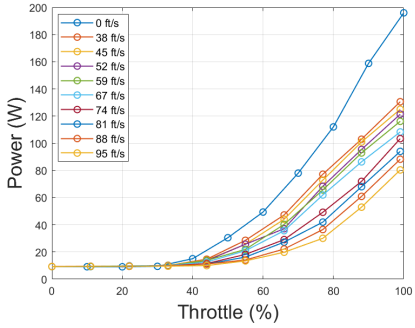

(c) Power vs. Throttle

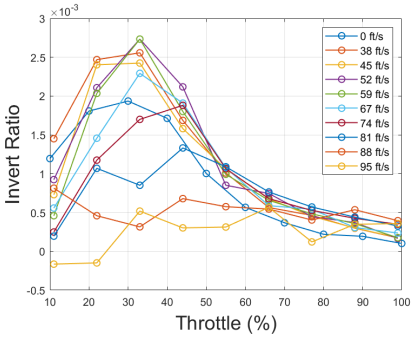

(d) Invert Ratio vs. Throttle

Figure 7: Single Propeller Testing Results

Comparing the Invert Ratios of each configuration helped to shine light on the optimal regions of operation, which could be adjusted downstream in the development process should more control authority or less power draw prove necessary. The results described in Figure 7d seemed to suggest the highest control authority per power requirement lived around ≈30% baseline throttle in wind speeds up to 74 feet/sec. While higher descent rates proved less responsive to the 30% baseline throttle, it was chosen as a good starting point to move forward with for further testing.

3.1.3 Conclusions

Single propeller wind tunnel testing focused on the potential viability of inverted control, by simulating the inverted environment in an experimental setting. The potential for control was analyzed through the motor's ability to affect drag, and the potential for decreased current draw on the motor.

The experiments described were successful on both accounts, showing promise for an inverted descent system to provide adequate control authority, as well as diminished power requirement. Results showed a ″sweet spot″ region of baseline throttle of ≈30% to be applied when inverted, that allowed for the maximum control authority per power draw on the motor in a majority of expected wind speeds. The results from this experiment helped inform further study of inverted descent, by providing a clear picture of the first principles of the system of inverted descent.

3.2 Bi–Rotor Testing

3.2.1 Ziegler Nichols Tuning Method

As previously mentioned, there is little to no research regarding the dynamics of inverted quadrotor descent. Should a mathematical model of a system be available, the parameters of the controller can be explicitly determined. However, when a mathematical model is unavailable, the parameters must be determined experimentally [14]. Ziegler Nichols (ZN) Tuning Method resolves this issue, providing a series of steps that can provide good estimates of gains based on empirically derived rules. In the case of the Inverted Descent Quadrotor, these gains can then be iteratively tested and improved but

provide a good starting point.

While closed and open loop methods of Ziegler Nichols exist, the closed loop tuning was deemed more appropriate due to potential nonlinearities due to the box housing used to test the bi–rotor system. Flow was not fully developed at the point of testing due to space constraints as shown in Figure 9. When holding an angle, this issue was compounded by the fact that one motor would be located in cleaner, more developed flow situated further from the intake. The other motor contrarily would be positioned in more turbulent air closer to the intake.

A further challenge was recognized due to potential ″ground effects″, explored in greater depth in [15], that were a result of the box housing shown in Figure 10. Holding an attitude resulted in one motor coming in closer proximity to the housing wall and the other motor gaining more distance away from the closest wall. With these potential nonlinear regions in mind, the tuning would ideally be performed in relatively the same positions that testing would occur, which made the ZN closed loop method a better candidate.

The first step of the ZN closed loop tuning method consisted of increasing proportional gain, until steady state oscillation occurred. This response was recorded, then the period of oscillation and proportional (ultimate) gain was identified. Using the period of oscillation and ultimate gain, recommended values were then calculated as described in Table 3 [14].

Table 3: Ziegler Nichols Gains

Control Type	K_p	T_i	T_d	K_i	K_d
P	$0.5K_u$	–	–	–	–
PI	$0.45K_u$	$0.8T_u$	–	$0.54^{K_u/T_u}$	–
PD	$0.8K_u$	–	$0.125T_u$	–	$0.1K_uT_u$
PID	$0.6K_u$	$0.5T_u$	$0.125T_u$	$1.2^{K_u/T_u}$	$0.075K_uT_u$

3.2.2 Cascade Control

Cascade control, shown in Figure 8 [16], provides an easily implemented control structure that can have improved disturbance response [17]. In the context of the bi–rotor experiment, attitude control was cascaded to rate control of the system. This structure complied with general rule of thumb for cascade control, which requires that the ″inner loop is faster than the outer loop. The secondary process must react to the secondary controller′s efforts at least three or four times faster than the primary process reacts to the primary controller. This allows the secondary controller enough time to compensate for inner loop disturbances before they can affect the primary process″ [17].

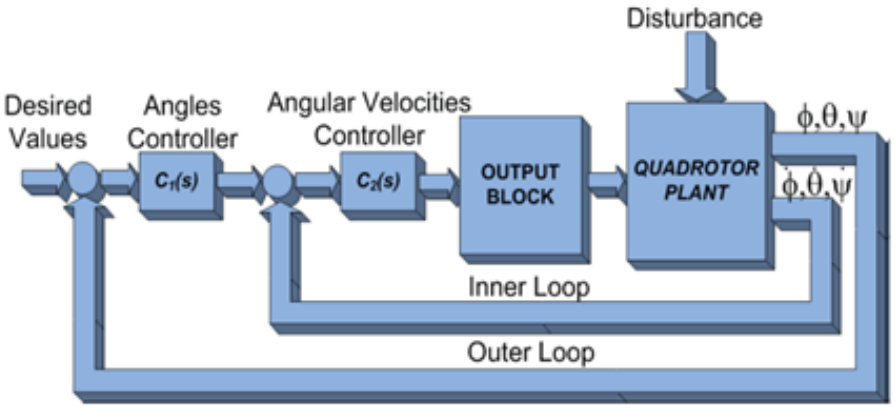

Figure 8: Cascade Control Structure of Quadrotor

Attitude estimates for the bi-rotor system were measured from the absolute rotary encoder, then subtracted from the desired set points mapped to RC stick inputs to yield an error signal. This error signal was scaled into a desired rate set point, then converted to rate error signal by subtracting the smoothed gyro z reading from the Raspberry Pi 3. This rate error signal could then drive motor commands to minimize error in the system. In general, tuning of the innermost system should occur first, followed by outer loops [18], a guideline that was followed in the bi–rotor experiment.

3.2.3 Methods

3.2.3.1 Physical Setup

Since the test section area was too small to fit a bi–rotor system to scale, a custom box was used to house the bi-rotor at the intake of the wind tunnel. The wind tunnel drew in air from the end of the box, and past the bi–rotor stationed 2 feet downwind. As previously stated, the airflow did not have enough room to become fully developed due to space constraints and was limited to a maximum of 47 feet/sec due to the increased intake size to fit the bi–rotor. While this did not accurately reflect the estimated terminal velocity of inverted descent ($\sim$88 ft/s), it was deemed acceptable for a proof of concept for which the bi–rotor was intended.

Figure 9: Bi–Rotor Test Setup

The bi–rotor was allowed one degree of freedom, rotating in roll about a shaft and bearing assembly mounted to the 90 degree load cell as seen in Figure 9. The load cell measured parallel and perpendicular drag components relative to wind direction, allowing for glide estimation using Equation 5.2. The testing also yielded an estimation of the Drag Area of the aircraft based on Equation 3.5, that could inform the expected terminal velocity of the aircraft.

$$Glide = \frac{F_{\perp}}{F_{\parallel}} \tag{3.4}$$

$$F_D = 0.5 C_D A \rho V^2 \tag{3.5}$$

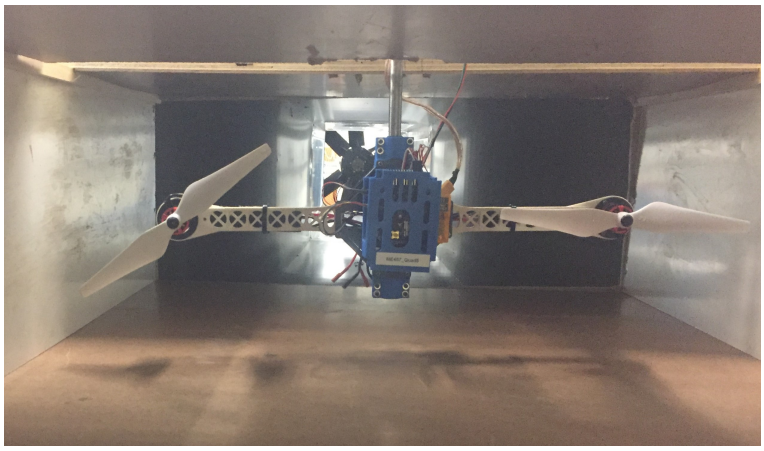

Figure 10: Bi–Rotor

The bi–rotor itself, shown in Figure 10, consisted of a standard F450 frame with two arms, ESCs, 9″ propellers and 920 kV motors. The center of the frame had custom 3d printed housing to clamp the shaft extending through the body. All control was performed with the same Raspberry Pi 3, Navio2 Autopilot and Spektrum Transmitter/Receiver setup used in Single Prop testing. Current load was monitored using the ADC power port for the Navio2. The ADC port measured both voltage and current draw through a power module, which could be used for power calculation. The ADC2 port was connected to the absolute rotary encoder, making cascade control possible by providing an accurate attitude estimate. The associated wiring can be seen in greater detail in Figure 11

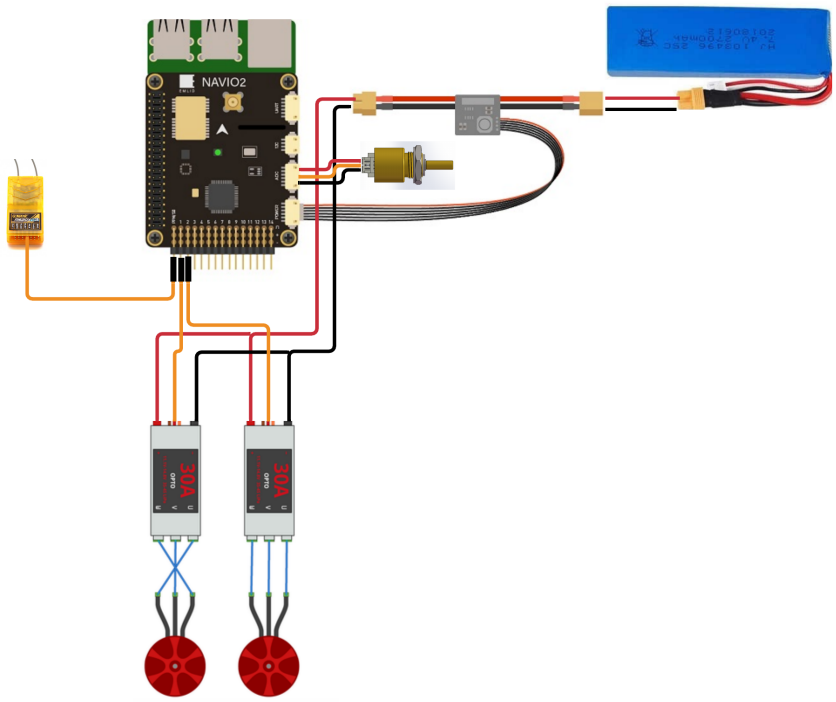

Figure 11: Bi–Rotor Wiring Diagram

3.2.3.2 Test Procedure

The ZN Closed Loop Tuning process, adapted to the needs of the bi–rotor system, began by instituting a closed loop, proportional rate controller. A 30% baseline throttle was applied as informed by the single prop experiment, and wind was brought up to its maximum 47 feet/sec. The system was held at 0 degrees, then released to observe behavior.

The proportional gain of the rate controller was then raised until steady state oscillation was observed. From the response, values for proportional, derivative, and integral gains could be experimentally derived for the rate controller. The values were tested by

performing a manual disturbance on the bi–rotor. The wind was brought up to 47 ft/s while holding a 0 deg/sec set point and a disturbance was induced by sharply twisting the shaft. Once this response was deemed acceptable, these values were then used for the inner loop of the cascade controller, and the focus on tuning was shifted to the outer, angle loop.

When efforts to tune the outer loop using the ZN process were unsuccessful, the outer loop was tuned using an iterative approach. This consisted of raising the proportional gain of the controller until oscillation was seen and then raising derivative gains to quiet this oscillatory behavior. Once relatively adequate control was achievable, the controller was tested with sets of -20, 0 and 20 degree commands in series to validate transient response.

After sufficient transient response was seen, the bi–rotor testing focused on identifying steady state performance metrics of attitude error, power, and glide ratio. The bi–rotor held angles of 0–30 degrees in steps of 10 degrees for $\approx$10 second intervals. Angles of greater than 30 degrees resulted in loss of control, due to wind vaning. In theory a 45 degree set point would be ideal for glide performance, however, due to these performance limitations angles greater than 30 degrees were omitted. Results regarding attitude error, power, and glide ratio could be evaluated and scaled to predict the behavior of the full inverted system and its potential benefits or shortcomings.

3.2.4 Results

With 47 feet/sec winds, the bi-rotor rate controller yielded steady state oscillation occurred at an ultimate gain of 2.0. The period of this oscillation was calculated to 0.375 seconds as seen in Figure 12 and Table 4.

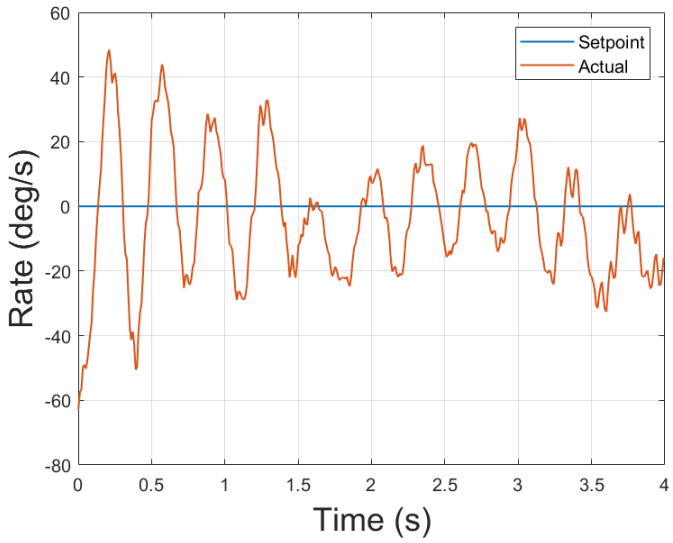

Figure 12: Ziegler Nichols Closed Loop Steady State Oscillations

Table 4: Ziegler Nichols Parameters

K_u	T_u
2.0	0.375

These values could then be used to estimate gains for different types of PID control. PD control, using only proportional and derivative terms, was chosen based on experiments with each type. Integral control was neglected due to control issues seen when attempting to implement an integral gain. An integral control term, regardless of how

small, seemed to result in negative performance, and complicated the process of iteratively improving the controller after ZN was performed. Table 5 summarizes the final gains of the rate controller.

Table 5: Ziegler Nichols Gains

Control Type	K_p	T_i	T_d	K_i	K_d
P	1.0	–	–	–	–
PI	0.9	0.31	–	2.88	–
PD	**1.6**	–	**0.047**	**–**	**0.056**
PID	1.2	0.188	0.047	6.4	0.056

Once seemingly controllable and stable, the Ziegler Nichols tuned rate controller′s performance was then tested by bringing the wind up to 47 feet/sec, while the bi–rotor held a 0 deg/s set point. A manual disturbance was initiated, by twisting the shaft by hand. While the performance metrics shown in Table 6 were not ideal, efforts for improving performance iteratively were generally unsuccessful. The performance, shown in Figure 13, was deemed acceptable to move forward with and implement into a cascade control structure.

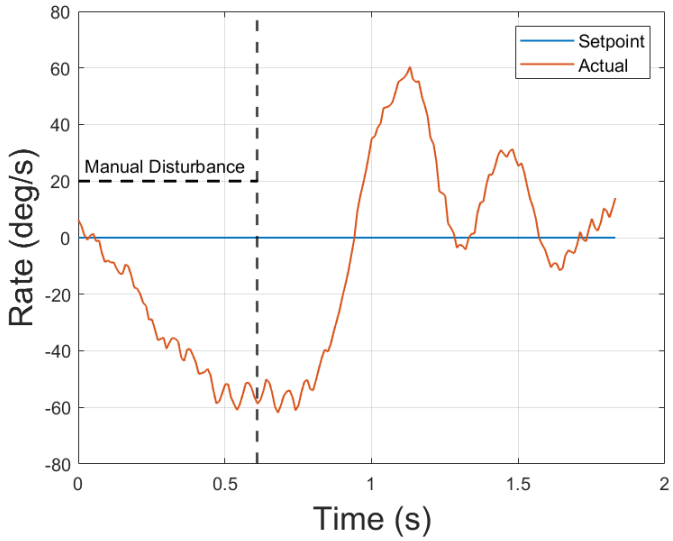

Figure 13: Ziegler Nichols Tuned Rate Controller Performance

Table 6: Rate Controller Performance Metrics

Metric	Value
Rise Time (T_r)	0.17 s
Peak Time (T_p)	0.371 s
Percent Overshoot (% OS)	107 %

After implementing the cascade controller, consisting of attitude control fed into the Ziegler Nichols tuned rate controller, the bi–rotor was capable of holding attitude set points even under the 47 feet/sec simulated descent conditions. The outer control loop again consisted of PD control, tuned iteratively to the final values shown in Table 7.

Table 7: Bi–Rotor Cascade Controller Gains

Controller	Gain	Value
Rate	P	1.6
Rate	D	.05625
Angle	P	2.25
Angle	D	0.07

Performance was tested at 47 feet/sec wind conditions, with the series of input commands shown in Figure 14 to test the transient performance of the controller. The response showed promise, displaying the ability of the bi–rotor to overcome the challenges associated with high wind velocity and track attitude set points. While the transient and steady state performance, summarized through the metrics listed in Table 8, did not yield quality performance, it was deemed satisfactory for a proof of concept and to move forward with further testing.

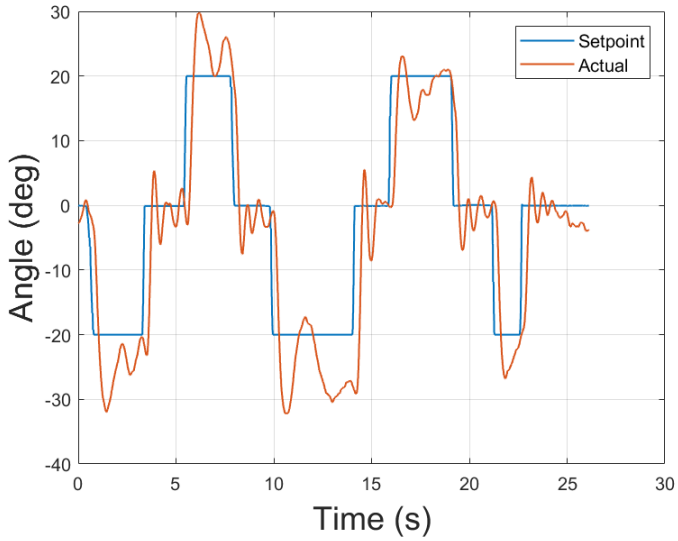

Figure 14: Cascade Controller Transient Performance

Table 8: Cascade Controller Performance Metrics

Metric	Value
Rise Time (T_r)	0.19 s
Peak Time (T_p)	0.303 s
Percent Overshoot (% OS)	37.2 %
Steady State Error	5.5 deg

Once the bi–rotor system could reliably hold different attitude set points, further testing was performed on steady state power consumption, glide performance and attitude control. Desired set points of 0 – 30 degrees were commanded in 10 degree steps, and power, glide and attitude data was logged for ≈10 second intervals.

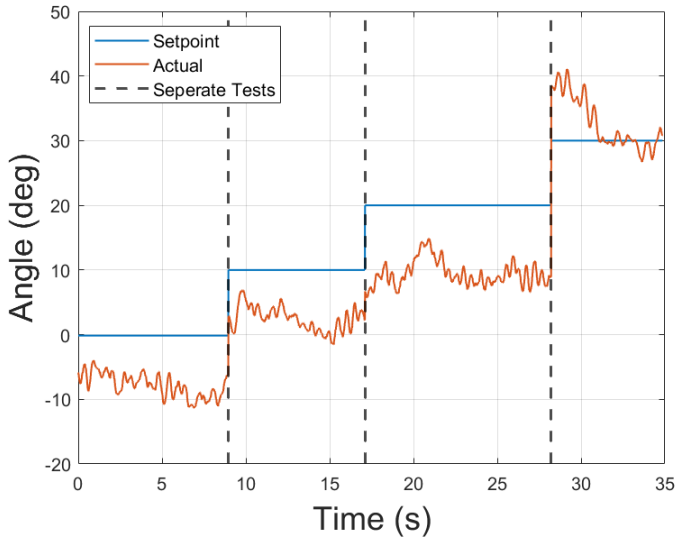

Figure 15: Cascade Controller Steady State

The inability of the controller to overcome a $\sim$10 degree bias was clear from the results shown in Figure 15. Efforts to mitigate this steady state error by implementing an integral term led to integrator windup resulting in diminished transient performance. The bias seemed to stem from the naturally stable position of descent, driven by the geometry of the bi–rotor system. However, the difference between the steady state performance of the system at the 30 degree configuration seemed to suggest that the housing and turbulent airflow did in fact induce non linear effects on the system, which could explain some of the performance issues seen by the bi–rotor.

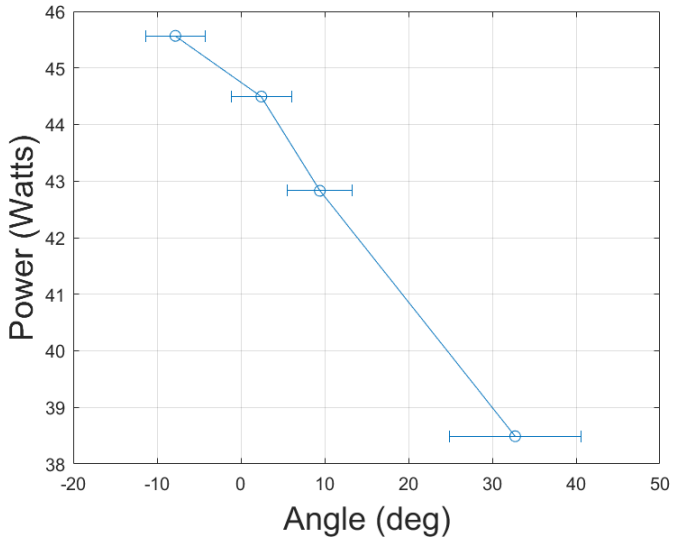

Figure 16: Bi–Rotor Power vs. Angle

The resulting power consumption from the bi–rotor system was encouraging as seen in Figure 16. The system showed promise for substantial energy savings when scaled to a full quadrotor system. It tied in nicely with the results from single propeller wind tunnel testing, where 30% throttle power resulted in roughly 10 Watts of power requirement, which scaled reasonably well to the $\sim$42 Watts seen from the bi–rotor system. Glide performance was also characterized, quantifying the potential ability of the inverted descent system to translate and track waypoints while inverted as illustrated in Figure 17.

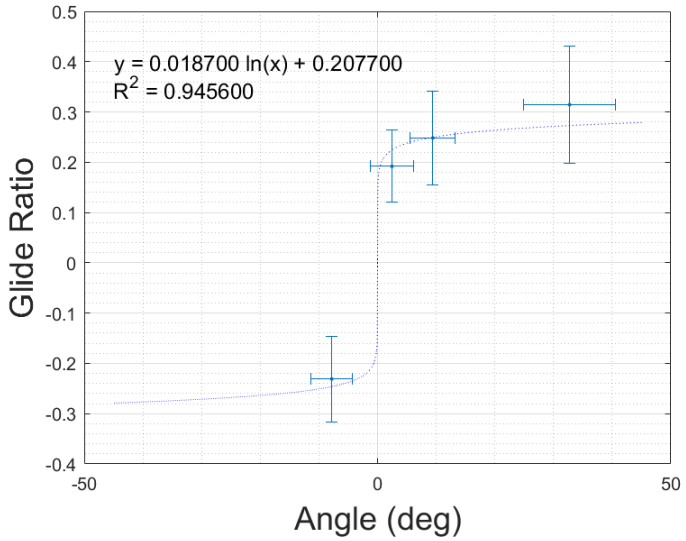

Figure 17: Bi–Rotor Glide Performance

$$GR(\theta) = 0.0187ln(\theta) + 0.208 \tag{3.6}$$

$$R^2 = 0.95 \tag{3.7}$$

The glide performance of the bi–rotor suggested the potential for adequate translational capabilities when applied to a full scale system. While a glide ratio of $\sim$0.3 may not be sizable when compared to aircrafts in general, it would provide ample translational capability in descent, and the ability to fight substantial winds to maintain trajectory.

Table 9: Estimated Aerodynamic Properties

Metric	Value
Drag Area (C_dA)	0.0186
Terminal Velocity	58.29 ft/s

The resulting drag force from wind tunnel testing gave estimates for the drag area of the vehicle and the corresponding terminal velocity show in Table 9 that were derived using Equation 3.5. These metrics gave further information as to the speeds of operation that could be taken into account when referring back to single propeller testing and validated the choice of a 30% baseline throttle moving forward.

3.2.5 Conclusions

While the bi–rotor system provided a valuable proof of concept and showed potential for control in 1 axis at near inverted speeds, the tuning process and resulting controller performance were less than ideal. A severe attitude bias in the system prevented integral control from being added, which diminished steady state performance due to the inability to control steady state error.

Space constraints resulted in testing the bi–rotor in underdeveloped flow, which likely was the cause of severe perturbations and buffeting. The system required testing at what was assumed to be less than terminal velocity, due to the limitations of the wind tunnel available for testing. The housing surrounding the system also introduced potential non–linearities from ground effects due to the side walls.

With these limitations in mind, the bi–rotor system validated the potential for transient and steady state control of inverted descent, and yielded valuable gain tuning values that could inform a potential full scale system. Even with the challenges of housing induced nonlinearities and potentially turbulent flow, the bi–rotor was successful to a certain degree of controlling attitude which generated translational forces for glide. The

system achieved this control with a predictably low power draw, which further validated the expectation of decreased energy for descent when scaled into a functional inverted descent system.

CHAPTER 4

FULL SYSTEM BASELINE THROTTLE TESTING

After gaining a deeper understanding of inverted descent through wind tunnel testing, a full scale Inverted Descent Quadrotor was designed and implemented. To validate functionality, as well as help further identify the ideal ″baseline throttle″, a series of tests were performed at Swope Park which allowed for flights up to 400′ AGL. While the descents were brief ($\sim$5 sec) informative data and meaningful conclusions were drawn regarding the ideal baseline throttle of the inverted descent system.

4.1 Methods

4.1.1 PX4 Build

4.1.1.1 Hardware

The build for the inverted descent drone began with the Pixhawk 2.1 Cube Black flashed with PX4 firmware as the flight controller. The system was setup in a Quad+ Airframe configuration, to preserve the geometry of the bi–rotor setup tested in the wind tunnel. The quadrotor utilized standard 30A ESC′s, 920kV brushless motors, and 9″ propellers as depicted in Figure 18.

Figure 18: Inverted Descent Quadrotor

The additional sensors and peripherals used were vital to the testing, as later experiments were performed at altitudes high enough to render normal range RC inadequate, as well as to make visual flight control nearly impossible. A Here2 GPS module was used as primary GPS. The RFD 900+ Modem received RC control input coming from the FrSky Taranis QX7 transmitter fitted with RFD TX–Mod Transmitter module. This pairing, presented in Figure 19 allowed for long range RC control over 40 km, as well as broadcasting telemetry back to a Ground Station via Wifi bridge. The ground station consisted of a laptop running QGroundControl, allowing for position, battery, altitude, and other vital data to be monitored in real time from the quadrotor.

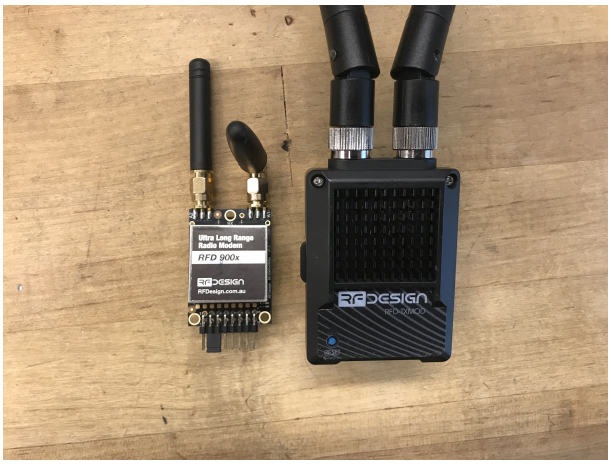

Figure 19: RFD Transmitter and Receiver Pair

4.1.1.2 PX4 Control Structure

PX4 is a widely used, open source control software compatible with several autonomous airframes, chosen for its reliable performance and variety of control modes available for the inverted descent system. In the PX4 multirotor airframe, there proved to be 3 important modes of interest when implementing inverted descent for testing.

The control structure of PX4 resembles an extended version of the cascaded controller seen in the bi–rotor testing phase, depicted in Figure 8. The structure, visible in Figure 20 consists of the same attitude control cascaded to rate control, however, has additional position control cascaded to body velocity upstream of attitude control. This structure allows the pilot to select a variety of control regimes by simply changing modes.

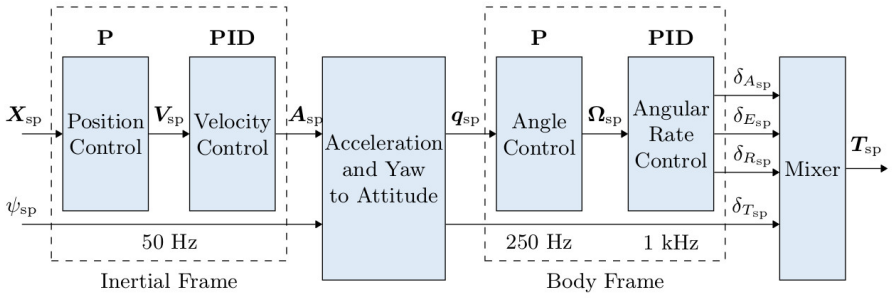

Figure 20: PX4 Control Architecture

The first important mode utilized in the descent testing was Position Mode. Described as an ″Assisted″ flight mode, the multirotor controls xyz body velocity using GPS measurements and will fight wind to maintain GPS coordinate lock. Roll and pitch commands correspond to new GPS set points, and throttle inputs control climb/descent rates. This mode was used in the ascent phase of testing, as well as the ″recovery″ phase. Autonomous flight allowed for more focus on telemetry output at Ground Station during ascent, to ensure the maximum altitude of testing location was not exceeded.

The ″recovery″ phase consisted of flipping to Position Mode after inverted descent which resulted in the quad flipping back over to its normal orientation and throttling up to end rapid descent. Position Mode′s body velocity control worked well for this phase, as thrust was increased automatically to end rapid descent, but then backed off once the quad reached a stabilized hover again.

Manual mode was another vital control mode used in descent testing. The manual control mode passes roll/pitch inputs as attitude set points, yaw inputs as rate set points, and throttle passed directly to output mixer. This mode was ″hijacked″ for inverted descent, as described later.

The final control mode of importance was Altitude mode, which passed roll/pitch/yaw commands as described in Manual mode, however mapped throttle inputs to climb/descend at predetermined maximum rates. Center throttle hold altitude steady, allowing for drift in xy due to wind. This mode was utilized in the normal descent configurations, as described in Chapter 5.

4.1.1.3 Software Changes

To successfully implement inverted descent into the PX4 framework, a series of changes were required in the flight stack as summarized in Table 10. All changes were made to the latest stable release of PX4, which at the time was v1.11.02.

The first change was to add 180 degrees to the roll attitude set point when in Manual control mode. The manual mode now corresponded to the ″Inverted Descent″ mode. The appropriate baseline throttle, empirically derived from testing, was set to the throttle command, again while in manual mode. This value was fixed, and throttle stick position no longer affected throttle input.

A series of new parameters were also created, to serve as the inverted gains when in manual mode for roll, pitch, yaw rate and attitude. The software was adjusted to use these gains when in manual mode, rather than the normal flight gains. These inverted gains were scaled from values derived from wind tunnel bi–rotor testing.

The yaw gains for rate and attitude were reversed due to the reversal of yaw control direction when inverted, as discussed earlier. Because no yaw tuning could be completed in the bi–rotor experiment, yaw gains were left with the same magnitude as the default

PX4 gains.

Table 10: PX4 Software Changes

Variable	Location	Change
attitude_setpoint.roll_body	mc_att_control_main.cpp	Add 180 deg and use Inverted Gains if in Manual Mode
throttle_stick_input	mc_att_control_main.cpp	Set to Baseline throttle if in Manual Mode
Roll/Pitch/Yaw Gains (Angle)	mc_att_control_main.hpp	Tuned Values (Reverse signs of Yaw)
manual_rate_setpoint	MulticopterRateControl.cpp	Use Inverted Gains if in Manual Mode
Roll/Pitch/Yaw Gains (Rate)	MulticopterRateControl.hpp	Tuned Values (Reverse signs of Yaw)
MPC_MAN_TILT_MAX	QGroundControl Parameters	Set to desired Maneuver
MPC_Z_VEL_MAX_DN	QGroundControl Parameters	Set to desired Descent Rate

Changes were also necessary for descent testing described in Chapter 5, in order to adjust maximum descent rate and maximum angle command for descent. Both items were changed via QGroundControl, and could be adjust on the fly for each test configuration. Adjusted maximum descent rate allowed for throttle to be set to zero when the mode was switched to altitude mode to trigger descent, and the descent rate would saturate at the set value. Adjusted maximum tilt angle allowed for a full roll/pitch stick to map to the required command for each configuration to simplify testing procedure.

4.1.2 Test Procedure

The baseline throttle testing consisted of an initial 4 flights, starting from 0% baseline throttle and incrementing in 10% steps up to 40% baseline throttle. The overall test procedure for each flight, summarized in Table 11, consisted of an ascent up to 400′ AGL, followed by a half flip triggering inverted descent, a series of roll/pitch maneuvers, and finally a recovery flip to arrest descent.

During descent, commands were given for a +/- 35 deg roll multistep, followed by the same in pitch. This maneuver, depicted in Figure 21, was used to characterize the

Table 11: Baseline Throttle Test Procedure

Order	Phase	Mode	Maneuver
1	Ascent	Position	None
2	Half Flip	Manual	180° Roll
3	Descent	Manual	Pitch/Roll Maneuvers
4	Recovery	Position	Half flip and arrest descent

control of each configuration. While including a yaw maneuver into the test would have yielded more results with which to compare, the descent time was too small to allow for a yaw maneuver, so it was assumed that testing the capability of the yaw controller to hold a zero set point throughout the flight was sufficient.

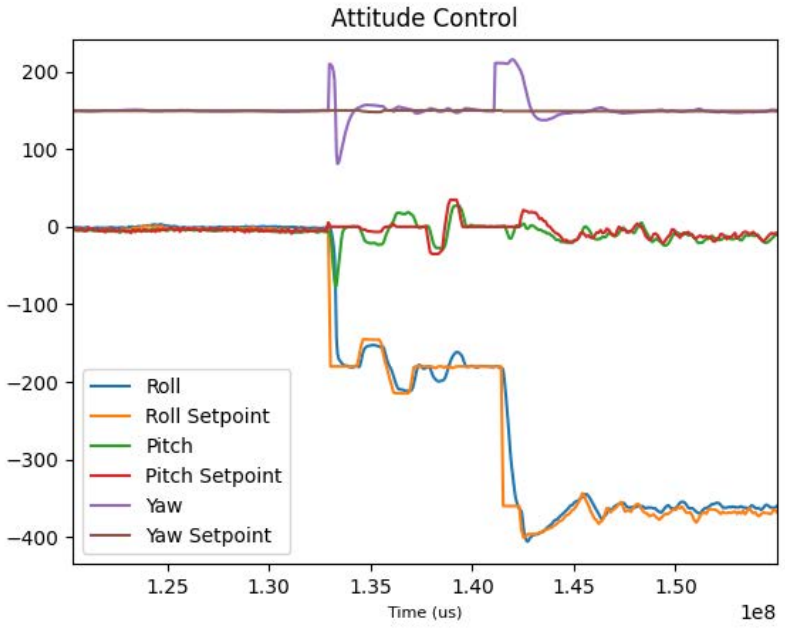

Figure 21: Baseline Throttle Test Maneuver

Results were parsed and compared again in 2 main categories, control, and power.

Each metric excluded the high dynamic, power hungry half flips, only taking into account the inverted descent of each test. Control was quantified by the Mean Average Error, described in Equation 4.1, over the descent for the roll, pitch, and yaw axes. Simple error was insufficient in quantifying control, as values oscillating around the set point would result in a mean of zero error. Power was calculated, again using Equation 3.2, and compared between configurations.

$$MeanAverageError(MAE) = mean(|\theta_{desired} - \theta_{actual}|) \tag{4.1}$$

4.2 Results

Testing the effects of baseline throttle on the Inverted Descent Quadrotor yielded results that provided further insight into how previous single prop and bi-rotor testing results scaled into a full scale system. As expected from previous experiments, increasing baseline throttle led to significant improvements in the system′s ability to track set points, apparent in Figure 22.

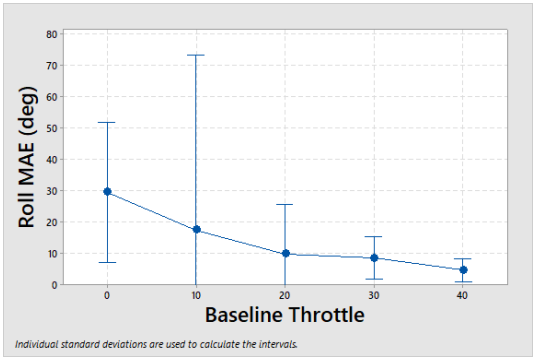

(a) Roll Angle MAE

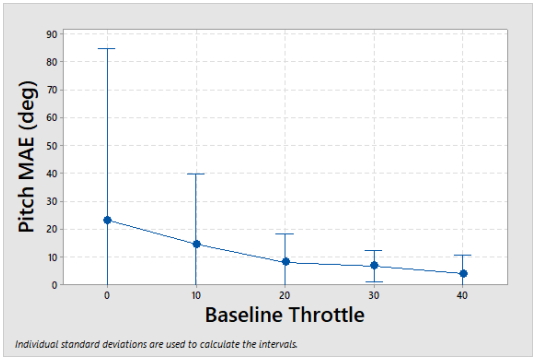

(b) Pitch Angle MAE

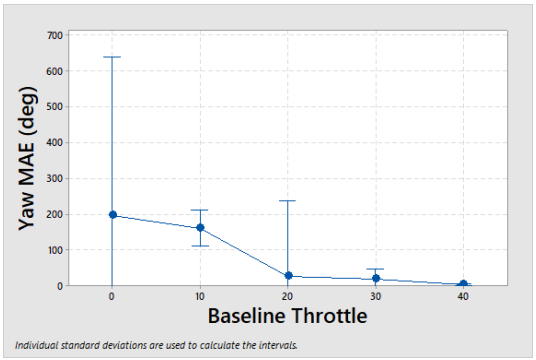

(c) Yaw Angle MAE

Figure 22: Attitude Performance vs. Baseline Throttle

Despite no wind tunnel tuning, yaw performance from Figure 22c proved to be superb with higher baseline throttle levels, suggesting that the system of inverted flight might be less dissimilar from normal flight than initially expected.

Power consumption results for each baseline throttle configuration were yet again, encouraging from Figure 23. The power was higher than expected from simply scaling the bi–rotor testing, likely due to the addition of a previously ignored control axis in yaw. The high power corresponding to the 0% and 10% configurations was assumed to be an

anomaly, as these configurations had no repetitions as shown in Table 19. Further testing would likely yield the same trend of decreasing power with decreasing baseline throttle seen from the other configurations.

The baseline testing results further validated the choice of 30% as a quality baseline throttle, as it yielded good attitude control without requiring excessive power like the wind tunnel testing suggested.

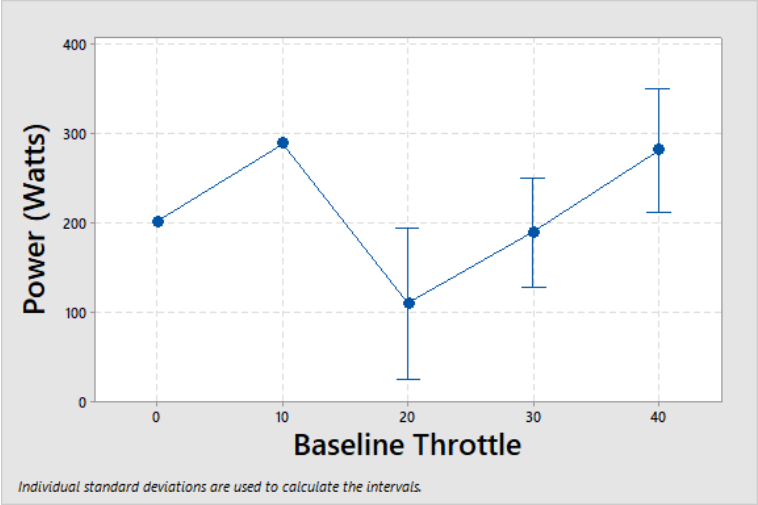

Figure 23: Baseline Throttle Power Results

4.3 Conclusions

Baseline throttle testing helped to validate functionality of the inverted descent system, give a cursory outlook on the performance, and build upon single prop and bi-rotor testing by further identifying the ideal baseline throttle for inverted descent. The 30% baseline throttle performed well, providing a high level of attitude control relative to power requirement. For this reason, it was chosen as the setting for subsequent descent

testing described in Chapter 5.

The assumption that too little baseline throttle would result in loss of control was legitimized, seen in the increasingly unstable roll, pitch and yaw performance of the 0% and 10% baseline throttle configurations. The experiment also confirmed the earlier assumption that diminishing marginal returns exist when increasing baseline throttle. When comparing the 30% and 40% configurations, it was clear that the relatively high change in power draw, resulted in relatively small improvements to attitude control.

The resulting power of the bi–rotor experiments did not scale as expected to the 4 motor, full scale system. The increase from expected power was likely due to the increased number of peripherals, such as GPS and long range telemetry modem. Adding yaw control to the system likely induced increased motor activity, which also could have been the culprit for greater than expected power requirements. Despite the higher than expected power, the Inverted Descent Quadrotor still showed promise moving forward into the full descent testing phase.

CHAPTER 5

DESCENT TESTING

Once an ideal baseline throttle was experimentally derived and basic functionality was proven, testing could move towards comparing the full scale inverted descent system to normal modes of descent. Performance of the inverted descent system was tested from 400′ up to 1,499′ AGL, then compared to normal descent to identify significant benefits and drawbacks of the inverted system. Testing allowed each configuration to be compared in control, power, velocity and translation/glide to rank performance, as well as provide meaningful data to be used for simulation of more realistic mission scenarios.

5.1 Methods

5.1.1 Test Procedure

Quantifying the performance of normal descent against inverted descent resembled the Full System Baseline Throttle experiment in many ways. The experiment used the same quadrotor hardware setup and assemblies, with the same software changes other than the baseline throttle being fixed to the 30% setting derived from the prior testing.

The goals of the testing were to approach Vortex Ring State in normal descent and quantify its effects on control, power and translation performance. The performance of normal descent could then be compared to inverted descent in the same metrics. Testing procedure followed the flowchart depicted in Figure 24. Normal descents were performed

in altitude mode, while inverted descents were triggered through manual mode. During the descent phase, a constant command of 0 – 30 degree incremented by 10 degrees was given during the duration of the descent, to help quantify control as well as translation/glide capabilities of each configuration.

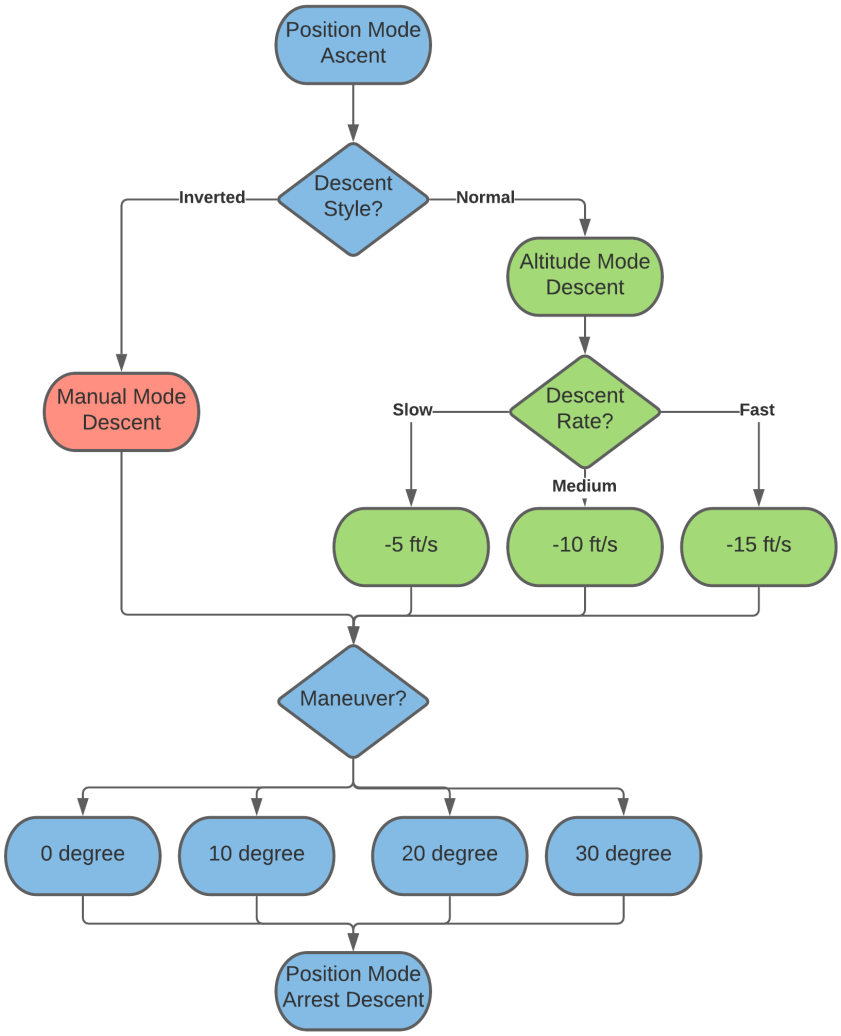

Figure 24: Descent Testing Procedure

Normal descent speeds were varied from -5 ft/sec to -15 ft/sec in steps of -5 ft/sec in an effort to approach and experience VRS. The VRS criterion was calculated with Equation 2.1 for the quadrotor system, suggesting that descent rates faster than -9.02 ft/sec would experience instability with no horizontal velocity. The slow descent rates of -5 ft/sec fall slower than the VRS minimum of -9.02 ft/sec, so no VRS effects would be expected for any -5 ft/sec descent configurations. With the default maximum translation velocity set to 39.37 ft/sec for a 35 degree default maximum set point in PX4, the expected relation with VRS was summarized through Table 12.

Table 12: Expected VRS for Normal Descents

V_z ft/s	$V_{H_{required}}$ (ft/s)	Maneuver (deg)	$V_{H_{expected}}$ (ft/s)	VRS?
-10	27.47	0	0	Yes
-10	27.47	10	11.25	Yes
-10	27.47	20	22.5	Yes
-10	27.47	30	33.75	No
-15	41.21	0	0	Yes
-15	41.21	10	11.25	Yes
-15	41.21	20	22.5	Yes
-15	41.21	30	33.75	Yes

To explore the effects of both descent style and maneuver on control, power and glide performance, a full factorial experiment was designed and performed. The factor of descent style had 4 levels, and the factor of Maneuver had 4 levels, as previously described. This resulted in 16 distinct configurations summarized in Table 20. Each configuration was at least tested at least once, however, some configurations had several repetitions due to logging or environmental issues as seen in Table 21.

Due to the far faster descent speeds of the inverted descent method, it was apparent that simply using power to compare the configurations would not tell the whole story. To consider the reduced descent time, total energy was calculated for each descent as seen in Equation 6.16, then divided by the total descent length.

$$Energy/_{ft} = \frac{\sum P_{inst}\Delta t}{\Delta Altitude} \tag{5.1}$$

For inverted configurations, the term ″glide″ was appropriate. The drag from descent drove translational movement, with a small thrust component from propellers acting in the opposite direction. For normal descent configurations the term ″glide″ was less appropriate, as power was being applied to induce a body velocity in the direction of flight. The desired comparison was between the capabilities of each configuration to translate during descent. To quantify this capability, Equation 5.2 took the magnitude of change in local position over the change in altitude in descent and termed the result ″glide″, despite not being correct in the literal sense of the word.

The glide metric did not take into account the direction of intended travel, only calculating the absolute distance from start to stop of the descent. This made the metric further susceptible to noise due to wind, however repetitions of configurations over several days, as described in Table 21 was assumed to account for this experimental noise.

$$GlideRatio = \frac{\sqrt{\Delta x_{pos}^2 + \Delta y_{pos}^2}}{\Delta Altitude} \tag{5.2}$$

As important as the metrics themselves, were the parts of flight over which these metrics were calculated. Roll, Pitch and Yaw MAE, along with power were calculated

from the ″steady descent″ phase of each flight, depicted in Figure 25. For inverted descents, steady state was defined as the phase of flight after the half flip to inverted descent mode was completed, taking ∼.85 sec, but before the recovery flip. For normal descent configurations, the steady descent phase was simply defined as the entire descent. This distinction was made to compare the steady state descent performance of each configuration while ignoring the high dynamic, high power, half flip maneuvers.

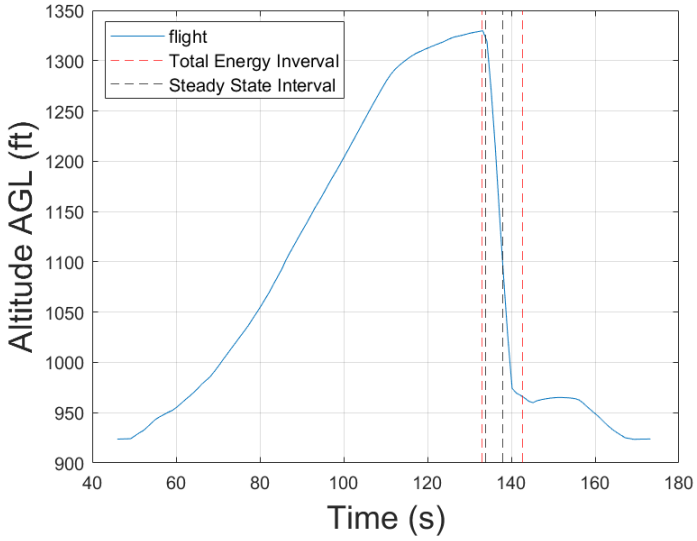

Figure 25: Areas of Descent for Calculations

Total descent energy, on the other hand, needed to account for the extra energy expenditure from the recovery flip. For this reason, energy calculations, reflected in the Energy/Feet metric, were calculated on the steady state descent, as well as an additional ∼4 sec window for inverted descent to allow the quad to arrest descent and regain stable flight as shown in Figure 25. All recovery flip analysis was performed on the same ∼4 sec window, which accounted for both the increased power to achieve the half flip, as well as

increased thrust to arrest descent and regain stable flight.

5.2 Results

When comparing control between differing descent styles, it was evident from Figure 26 that inverted descent held a higher degree of attitude control when compared to normal descent. In theory, as normal descent rates increased, control would decrease as the quadrotor would experience increasing effects from Vortex Ring State. Even when compared to the Slow descent configuration, Inverted descent showed improved roll, pitch and yaw control.

In normal descent, the descent rates chosen approached VRS with reasonable confidence, seen in the decreased attitude error from all normal descent rates at a 30 degree set point. The trend of increasing error with increasing maneuver magnitude, up until the 30 degree mark seemed to show the point that the quadrotor was translating out of VRS effects, before it was able to experience them.

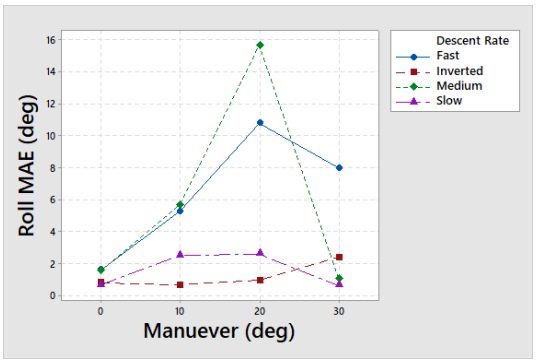

(a) Roll Angle MAE

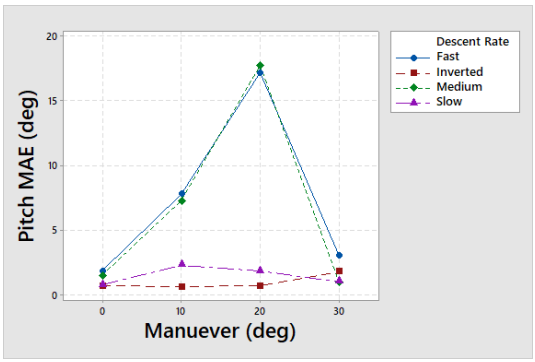

(b) Pitch Angle MAE

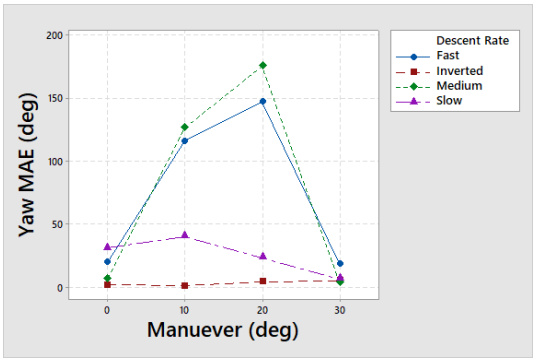

(c) Yaw Angle MAE

Figure 26: Attitude Performance of Descent Styles

When comparing power requirement and the associated energy consumption of each descent style in Figure 27a, inverted descent displayed power performance on par with the other methods. However, the increased velocity of descent resulted in remarkable efficiency for the Inverted case over other configurations, clear from Figure 27b.

The expected trend of increasing descent rates in the normal descent configuration resulting in decreasing energy was generally followed, as also shown in Figure 27b. However, there seemed to be an anomaly at the 20 degree configuration for both medium

and fast descents. When referencing back to Figure 26, it was clear that the 20 degree maneuver resulted in substantially higher attitude error for the medium and fast descent rates, suggesting that the increased energy and power could have been due to increased control actuation.

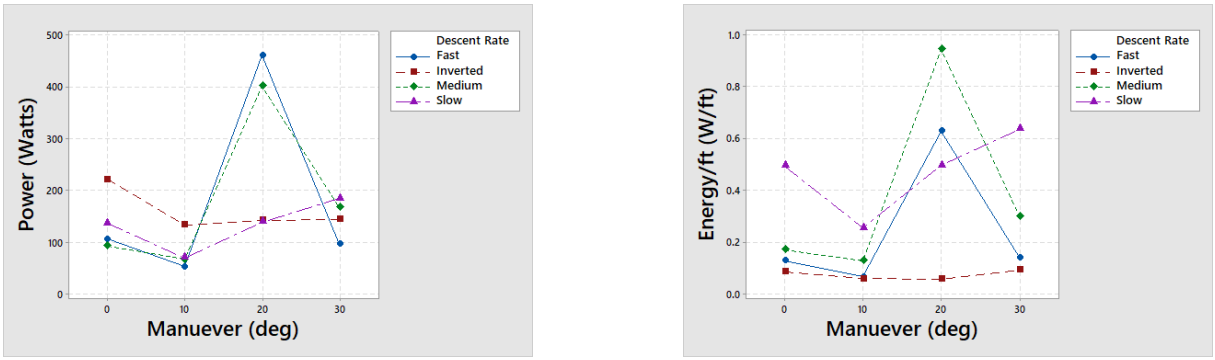

(a) Power vs. Descent Style

(b) Energy vs. Descent Style

Figure 27: Power and Energy Descent Testing Results

Translation/glide performance was more difficult to characterize, as wind conditions had significant effects on glide particularly for slower descent rates when the quadrotor took longer to descend and was exposed to prevailing winds for a longer duration of time. This fact explained the results shown in Figure 28a, with increasing bias for the 0 degree configuration as descent rate decreased, when in a closed environment with no wind a 0 degree set point should result in nearly no glide.

To resolve the inherent effects of wind on the data, the glide from each descent style was normalized by subtracting the 0 degree configuration bias from each maneuver for simulation. However, slower descents facing higher levels of exposure to winds, illustrated in Figure 28a, was an important trend to recognize moving forward into simulation.

Inverted descent showed much less glide performance than normal descent methods, and even less than was suggested glide performance from bi–rotor testing. It seemed that when compared to the bi–rotor system, the thrust generated from the two extra motors resulted in greater ″braking force″ that was not equally offset by increased drag from adding two more frame arms.

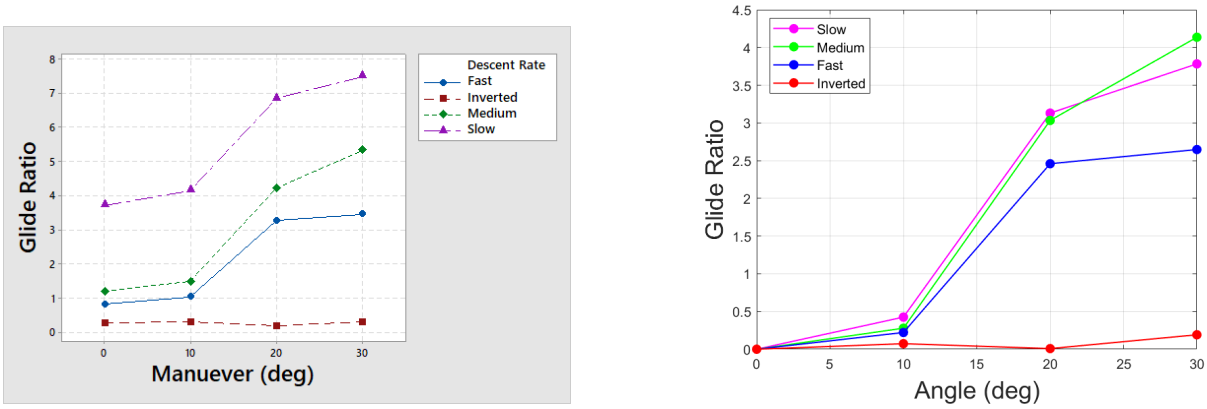

(a) Actual Glide Performance

(b) Normalized Glide Performance

Figure 28: Descent Testing Glide Results

The normal descents actual relationship with VRS for each maneuver could only be observed following testing. Slow descents were assumed to not encounter VRS as they fell slower than the -9.02 ft/sec minimum descent rate as previously calculated. The medium descents proved to experience VRS in the 0 degree and 10 degree configurations, as well as all fast descents. These results, summarized in Table 13, were close to what was expected and gave a good dataset to view the effects of VRS on normal descents.

Table 13: Realized VRS for Normal Descents

V_z ft/s	$V_{H_{required}}$ (ft/s)	Maneuver (deg)	$V_{H_{realized}}$ (ft/s)	VRS?
-10	27.47	0	0	Yes
-10	27.47	10	2.79	Yes
-10	27.47	20	30.33	No
-10	27.47	30	41.36	No
-15	41.21	0	0	Yes
-15	41.21	10	3.33	Yes
-15	41.21	20	36.89	Yes
-15	41.21	30	39.71	Yes

After testing the full test matrix of descent testing along with baseline throttle testing, 84 test flight had been performed, 45 of which were inverted descents. This relatively large dataset allowed for the identification of important flight characteristics, including terminal velocity and energy required for recovery flip maneuvers with relative confidence as seen in Figures 29 and 31.

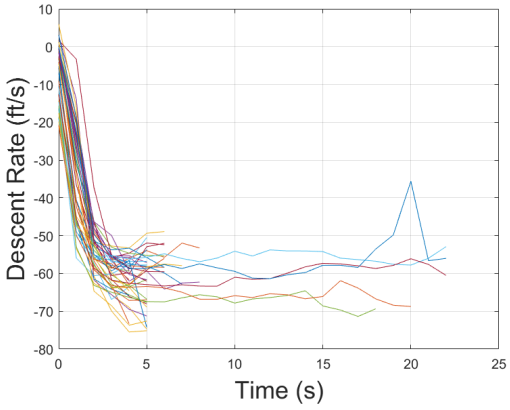

Figure 29: Terminal Velocity Results

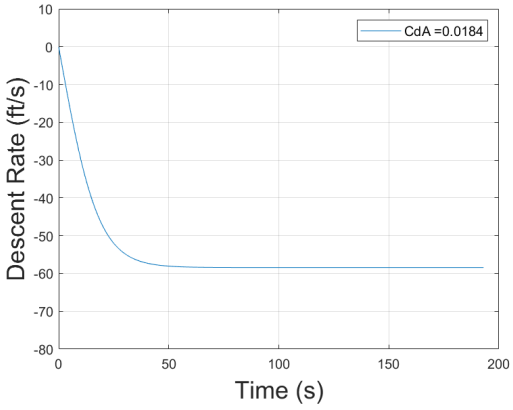

Figure 30: Drag Area Identification

From the terminal velocity descent analysis shown in Figure 29, an estimated terminal velocity of the quadrotor system was shown to be 58.65 ft/sec. This terminal velocity was within 1% of the estimated terminal velocity from bi-rotor experiments, giving increased confidence to the validity of conclusions and data from wind tunnel testing. The maximum wind tunnel velocity of 47 ft/s now more closely resembled that from terminal descent, again giving more merit to results from the bi–rotor experiment. With known air density, weight of the quadrotor, and the experimentally derived terminal velocity now readily available, the Drag Area of the Inverted Descent Quadrotor system could be calculated using Equation 3.5. The results of this calculation, shown in Figure 30, could then be implemented in later simulation.

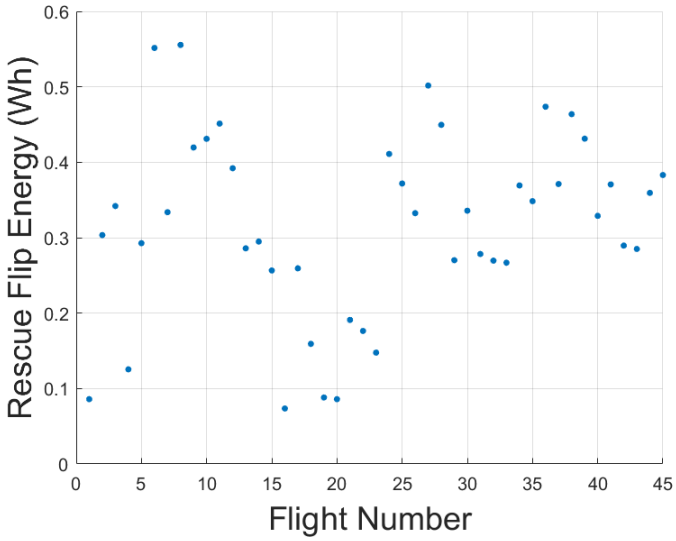

Figure 31: Recovery Flip Energy Requirement

Table 14: Recovery Flip Results

Average Energy (Whr)	σ (Whr)	95% Conf. Int (+/- Whr)
0.317	0.123	0.0368

Identifying a consistent energy of recovery flip maneuver allowed for simulation to take into account the increased energy to arrest the rapid inverted descent, using the values derived from Figure 31 and summarized in Table 14.

5.3 Conclusions

Valuable data was derived from descent testing that could then be leveraged into a simulation environment. Flight data regarding terminal velocity, recovery flip energy, and descent performance from the 16 tested configurations would prove invaluable moving

forward. Normal descents generally followed the trends expected, and the performance of the Inverted Descent Quadrotor was impressive in nearly every category.

Control in roll, pitch and yaw was substantially improved through inverted descent, on average yielding lower error than even slow descent. Steady state descent power requirements were generally equal, or even higher in inverted descent when compared to the normal descent methods, which was surprising. However, comparing the efficiency of the descent, using the metric of Energy/feet, showed a substantial improvement in Energy performance over normal descent methods.

Glide performance testing, on the other hand, yielded less promising results for inverted descent. The maximum glide ratio for inverted descent was roughly .19, occurring at the 30 degree maneuver as expected. This was well below the $\sim$0.3 glide ratio suggested from bi-rotor testing. While the inverted descent vehicle would still be functional, this low glide performance held potential implications when the descent system was evaluated from the mission level.

An inverted descent system with zero glide capabilities, for instance, would likely still be able to reach goal location of reasonable distance successfully, however, would have no ability to fight winds or translate towards goal during the descent. All translational movement would be delegated to after the descent, when the system could operate as a normal quadrotor at ground level. In this case there would be no reason for any baseline throttle, or possibly not even an active controller, as control of the quadrotor would not result in any useful work in the form of translation during descent, and only increase power requirements and energy consumption.

The glide of 0.19 observed from the experiments could likely be improved slightly with 45 degree set points, which were neglected from the test matrix due to issues with wind vaning in bi–rotor testing, however, were successfully achieved in descent testing. Regardless, even with a .19 glide ratio, an inverted descent system could be capable of fighting winds or translating in zero wind scenarios at a rate of 11.4 feet/sec ($\sim$ 7.77 mph). This performance suggests greater benefits from improving glide, rather than forsaking control altogether in an effort to decrease power.

With hard data to lean on, the development process moved into the simulation phase. Simulation would prove to further contextualize the potential of the Inverted Descent Quadrotor, and helped to compare this novel system to current PAD systems in industry.

CHAPTER 6

MISSION SIMULATION

With experimental data for power, attitude control, glide performance and velocity in the various descent configurations, results were extrapolated to further compare inverted descent to normal quad descent, as well as other precision delivery methods in more realistic scenarios than could be accessed for actual testing. In the simulated environment, comparison was made between methods of delivery in a variety of missions, wind conditions and payloads.

6.1 Methods

6.1.1 Mission Overview

Due to access and time constraints, testing of the inverted descent system was limited to basic descent testing, without realistic mission level phases. Real missions would consist of high-altitude deployment, then descent at a trajectory towards the goal location as depicted in Figure 32. The system would fight winds to the best of its ability, and track towards goal. After descent, should there still be distance to goal location, the quadrotor would resume normal flight towards goal.

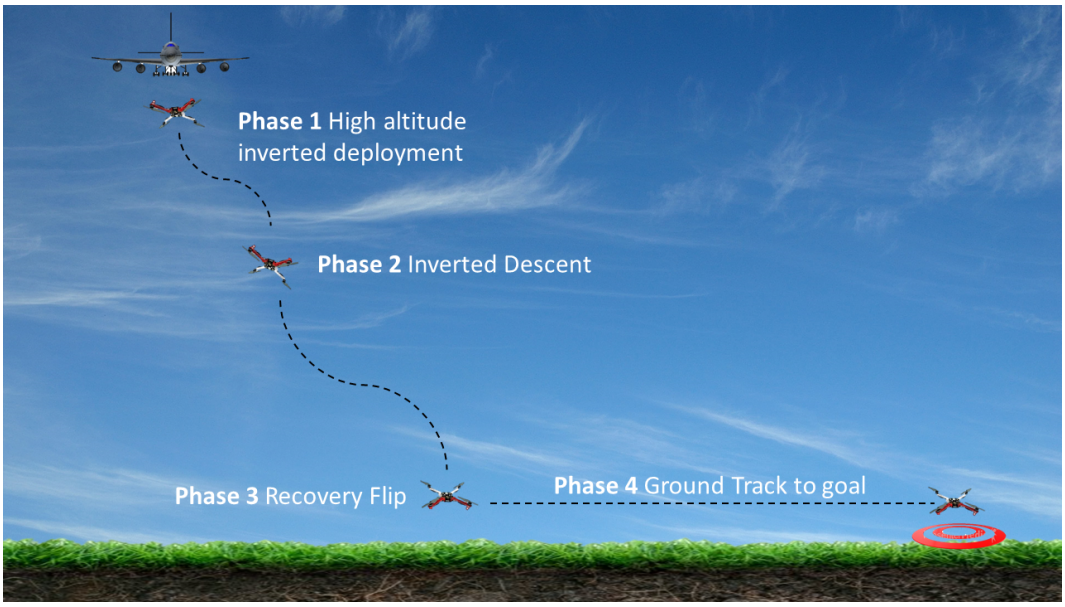

Figure 32: Mission Level Diagram

6.1.2 Ground Translational Test

The ground level translational phase of a mission would be a vital one, as the ability to translate once reaching ground displays the benefit of quadrotor systems over more traditional precision delivery systems. To accurately simulate mission performance, it was important to quantify both translational speed as well as power draw during the ground translation phase.

These metrics were quantified using the same quadrotor vehicle, with the translational speed parameter of PX4 set to its maximum of 65.62 feet/sec. Flights were performed at this speed, and power draw was logged, then averaged for a mean translational power of 421.69 Watts. While this was surely not the optimal translational speed with regard to power, these values were used in simulation. More extensive testing of energy

optimal translational speeds would result in improvements in ground level mission efficiency similar to [19].

6.1.3 Wind Conditions

In an effort to capture realistic wind conditions, data gathered in [20] was utilized from a series of balloon ascents and descents, from $\sim$4,500′ to $\sim$104,500′ MSL. These launches took place at various times on the same day, providing the ability to simulate predicted and actual wind data with various levels of accuracy. A good estimate (Type 1 fit) would correspond to predicted and actual wind data from the ascents of two balloons released at the same time. A medium estimate (Type 2 fit) could correspond to one ascent and one descent of balloons released at the same time. Bad estimates (Type 3 fit) could reflect balloons released at different times, in different phases of flight. Mean error was calculated for each potential combination of wind data, then bracketed into Type 1, 2, and 3 fits as summarized in Table 15.

Table 15: Wind Fit RMSE (ft/s)

Type 1	Type 2	Type 3
0 – 6.67	6.68 – 13.33	13.34 – 20

6.1.4 Simulation Steps

Simulation descent began by setting simulation parameters as defined in Table 16 for items such as deployment altitude, goal location, predicted wind data, and test wind data.

Table 16: Simulation Parameters

Parameter	Value
Deployment Altitude (MSL)	14500′
Ending Altitude (MSL)	4500′
Drag Area (C_dA)	.0184
Drone Weight M_d (lbs)	2.19
Battery Weight M_b (lbs)	0.47
Weight of Test System M_a (lbs)	2.66
Total Battery Energy (Whr)	34.04
Translational Power (W)	421.69
Translational Speed (ft/s)	65.62

For each configuration, the altitude descent simulation was performed at the corresponding descent rate. Normal descent methods′ descent rates were fixed to their initial values (–5, –10, –15 ft/s). Inverted descent began from rest, then accelerated to the terminal velocity identified experimentally. This compensated for changes of air density due to altitude in the inverted descent configuration. Altitude, descent velocity and acceleration were calculated at each time step until the configuration reached ground as shown in Equations 6.1 – 6.4.

$$m\ddot{z}_i = W - F_{drag} \tag{6.1}$$

$$\ddot{z}_i = g - \frac{C_d A \rho \dot{z}_{i-1}^2}{2m} \tag{6.2}$$

$$\dot{z}_i = \dot{z}_{i-1} + \ddot{z}_i \Delta t \tag{6.3}$$

$$z_i = z_{i-1} + \dot{z}_i \Delta t \tag{6.4}$$

During the descent phase, an ideal body velocity vector was calculated to reach goal location at the same time the quadrotor reached ground. This vector was adjusted at each time step to account for the predicted wind at the current altitude. The necessary calculations are described in Equations 6.5 – 6.11.

$$\theta_{goal} = \tan^{-} 1 \left(\frac{y_{goal} - y_{pos}}{x_{goal} - x_{pos}} \right) \tag{6.5}$$

$$d_{goal} = \sqrt{(y_{goal} - y_{pos})^2 + (x_{goal} - x_{pos})^2} \tag{6.6}$$

$$V_{t,goal} = \frac{d_{goal}}{t_{fromground}} \tag{6.7}$$

$$V_{x,wind} = V_{t,goal} \cos \theta_{goal} - wind_{pred,x} \tag{6.8}$$

$$V_{y,wind} = V_{t,goal} \sin \theta_{goal} - wind_{pred,y} \tag{6.9}$$

$$V_{t,goal,wind} = \sqrt{V_{x,wind}^2 + V_{y,wind}^2} \tag{6.10}$$

$$\theta_{goal,wind} = \tan^{-} 1 \left(\frac{V_{y,wind}}{V_{x,wind}} \right) \tag{6.11}$$

The simulation then interpolated the necessary glide/translation command to achieve the desired xy body velocity, given the current z velocity at each time step. If this glide/translation was unachievable for the configuration, the highest possible was chosen.

This desired glide/translation at each time step was mapped to a desired angle, based on experimental data from testing. The resulting actual angle was calculated using normally distributed error with a mean and standard deviation derived from the experimental descent testing results. The actual angle then corresponded to an actual glide/translation achieved and required power, both of which could be interpolated from empirical data. The xy position of the configuration was then updated for each time step from the actual velocity realized, based on the induced body velocity along with the actual wind data as calculated from Equations 6.12 and 6.13.

$$V_{x,actual} = glide_{actual}(-V_z)\cos\theta_{goal,wind} - wind_{actual,x} \tag{6.12}$$

$$V_{y,actual} = glide_{actual}(-V_z)\sin\theta_{goal,wind} - wind_{actual,y} \tag{6.13}$$

If the configuration was of normal descent style, a power multiplier was used to compensate for changes in the density of air, as well as potential increases in weight due to payload shown in Equation 6.14. Prior research had been performed investigating the validity of scaling power consumption at higher altitudes, and concluded that such scaling accurately reflected increases in power to an adequate level [21].

$$PowerMultiplier(c_{mult}) = \frac{m_2^{3/2}\rho_{test}^{1/2}}{m_{test}^{3/2}\rho_2^{1/2}} \tag{6.14}$$

$$Power_{scaled} = c_{mult} P_{interp} \tag{6.15}$$

$$Energy_{total} = \sum P_{scaled} \Delta t \tag{6.16}$$

Once the configuration reached ground, a fixed energy requirement of .317 W–hr was added to the total energy, only if the descent configuration was inverted. This fixed ″flip energy″ was derived experimentally from earlier testing, and was also scaled using Equation 6.14 for increases in payload or decreases in air density.

Now at ground level, if the configuration had still not reached goal location, it would induce a xy body velocity and power requirement that matched experimental data from translational testing in the wind adjusted direction of goal. The simulation would update xyz location, as well as total energy consumed until the configuration reached goal.

The distance from release point to goal location in the XY plane was described as standoff distance, for example a standoff distance of 0 ft would correspond to a release point directly above the goal location. The simulation iterated through 15 goal locations from 0 ft – 20,000 ft standoff distances and utilized every combination of predicted and actual wind data, keeping track of which Type of prediction each run fell into as visualized in Figure 33.

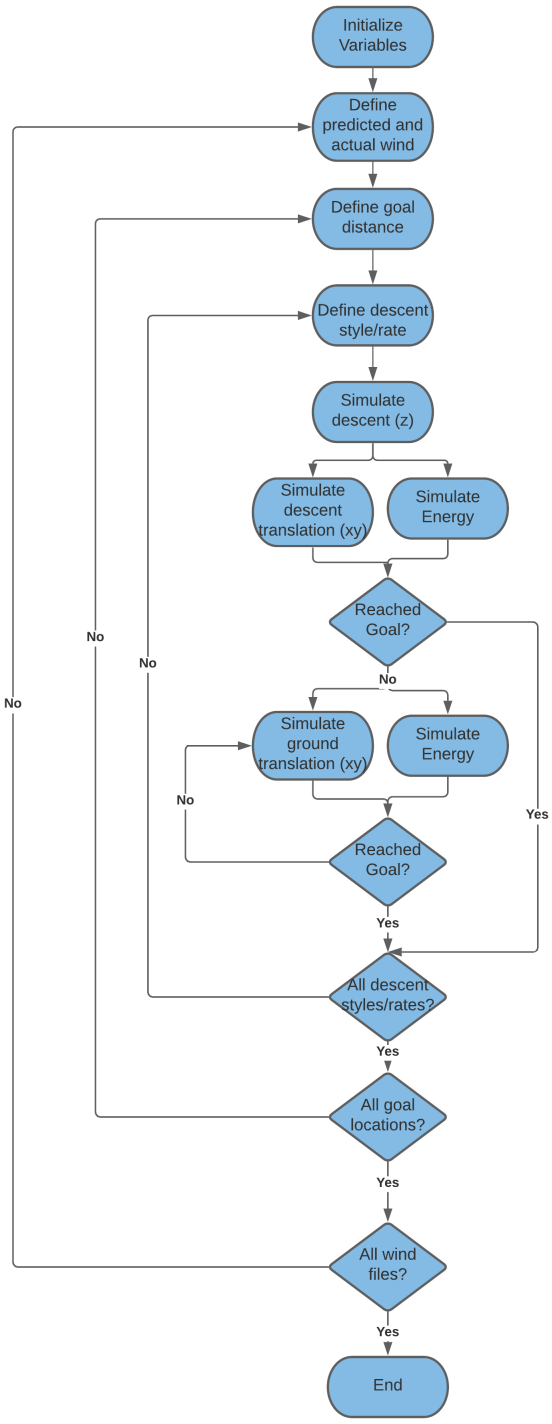

Figure 33: Simulation Flowchart

Simulating increasing payloads for all of the wind files helped to further illuminate the capability of the Inverted Descent Quadrotor. Thrust testing from the no wind case of the single propeller experiment showed the quadrotor system used to have a thrust capability of 9.89 lbs. This corresponded to a 3.72 thrust to weight ratio, which was implemented as the maximum simulation payload.

A maximum payload of $\sim$5 lbs would be closer to an optimistic estimate for the vehicle used in reality, to allow headroom for both the recovery flip rapid deceleration as well as control actuation. Further testing could help gain more confidence of payload capacity of this system. The same simulation flow was maintained as shown in Figure 33, while changing payload weights on the inverted descent configuration rather than changing descent style.

6.1.5 Assumptions

A few key assumptions were made in an effort to limit unnecessary work, without sacrificing the accuracy of the simulation. Terminal velocity was assumed constant, regardless of angle. While this is not true for inverted descent, it allowed for the z simulation to occur in its entirety before the xy simulation. Effects were deemed negligible as this assumption would only affect the inverted configuration and only in a conservative manner.

Yaw was ignored in the simulation, and it was assumed that the quadrotor was always pointed towards its desired heading. This assumption allowed empirical power data to be used in good faith. Although quadrotors are holonomic vehicles, power data was

gathered with one dimensional pitch set points and the effects of dividing these commands over two axes (roll/pitch) was unexplored, which could be an area for future work.

The battery capacity of the 4 cell 2300 mAh batteries used in testing were used as a benchmark to show how each method performed with respect to battery consumption as calculated in 6.17. It was assumed that these results could be scaled in a variety of ways to larger aircrafts, utilizing larger batteries. Battery percentage was simply used as a conceptual reference, to provide context to the less intuitive values of energy.

$$Energy_{batt}(Whr) = \frac{mAh(V)}{1000} \tag{6.17}$$

The assumption was made that as long as there was thrust headroom, any increase in payload would prolong the length of time of the recovery flip. This increased distance was assumed to be negligible when compared to the descent as a whole, despite the fact that there would certainly be natural limits for the system used. To maintain the same recovery flip seen in the system that was tested, the maximum payload was calculated to be roughly 0.5 lbs.

6.2 Results

Testing descent styles in a simulated environment yielded valuable insights as to how each configuration would perform, and if each configuration would be successful in different mission scenarios.

The trajectories of a single run of a Type I wind fit yielded verification of the simulation and showed an example of how wind interacts with each descent style as displayed

in Figure 34. Slow and medium descent rates were more affected by high winds due to the extended descent times. Fast descent resulted in the most direct trajectory, with less time exposed to high winds than slow or medium descents, and greater translational authority than Inverted descent. Inverted descent in this scenario resulted in the inability to hit goal during the descent phase, and ground tracking to goal after the recovery flip.

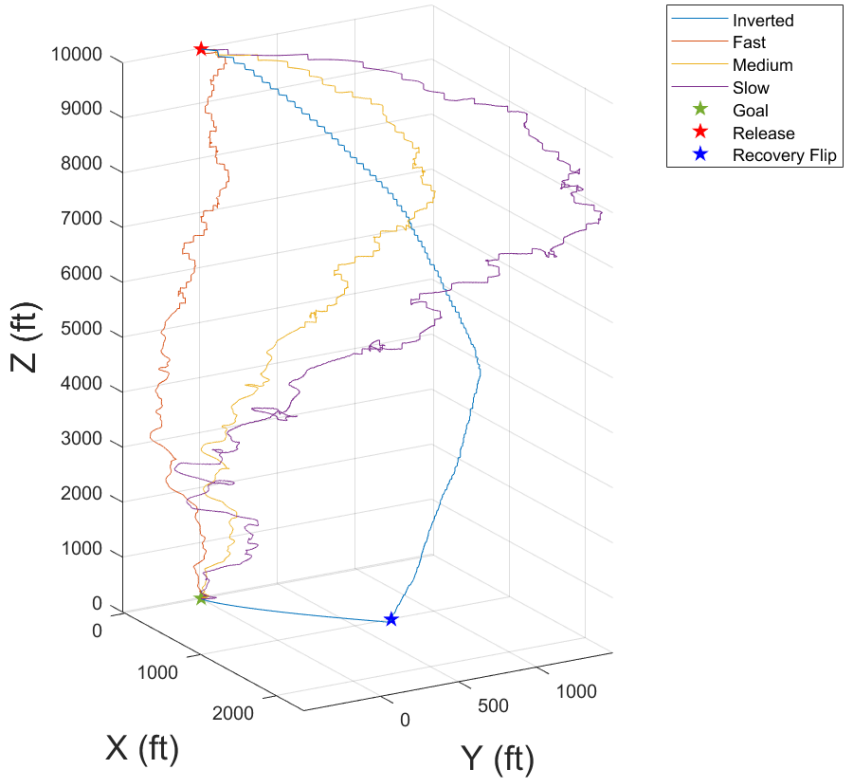

Figure 34: Simulation Example Trajectories

Again, Figure 34 helps visualize one descent simulation, but these simulations were averaged over the 91 wind combinations for each descent configuration, yielding the corresponding curves seen in Figure 35.

The results seen in Figure 35 helped highlight the benefits of inverted descent, as well as show why normal descent is not feasible for high altitude deployment. All normal descent configurations were unable to complete missions without an excess of energy over the battery capacity available, except for the fast descent in certain scenarios. While fast was narrowly capable of reaching goal without exceeding battery capacity in a few scenarios, the razor thin margin showed no potential for additional payload capacity.

The inverted descent configuration, on the other hand, proved capable of completing missions in a variety of wind conditions with adequate energy headroom to allow for additional payload. In the no payload case shown in Figure 35, inverted descent boasted translation potential for up to 17,975 ft when deployed from 10,000 ft. This translation potential, corresponding to a ″glide″ of 1.80 rivals that of current PAD systems, but with an unmatched level of precision and maneuverability.

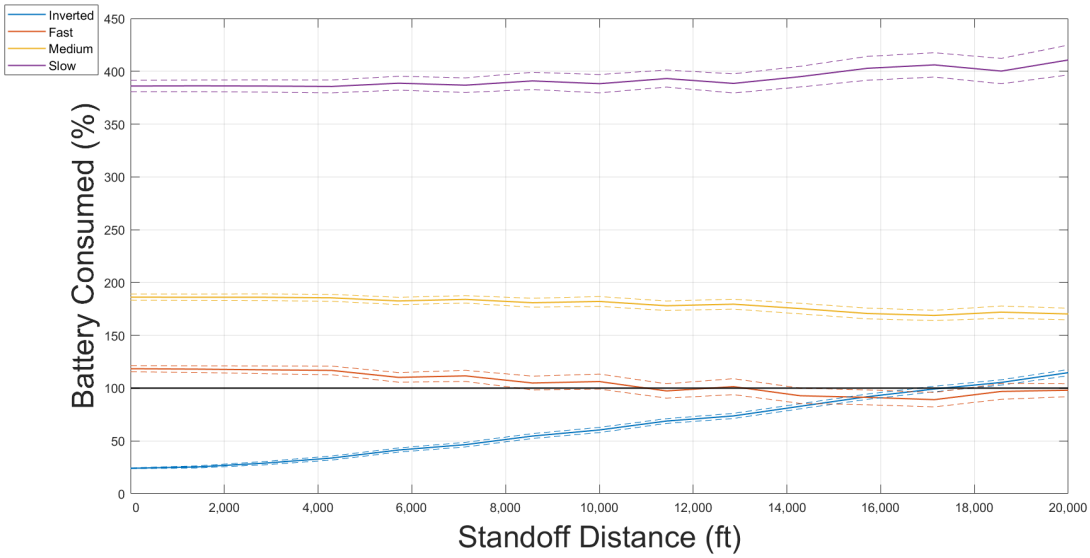

Figure 35: Descent Style Mission Comparison (95% Confidence)

As displayed in Figure 36, inverted descent proved to be quite robust with respect to quality of wind prediction due to the fact that a majority of translation occurs on the ground and faster descent rates leave less time for wind induced poor trajectories. Increasingly poor wind predictions only changed expected standoff potential by 676 ft. Compared to the other methods of PAD, whose performance have generally quite high sensitivity to wind prediction due to slow descent speeds, the Inverted Descent Quadrotor system showed substantial potential.

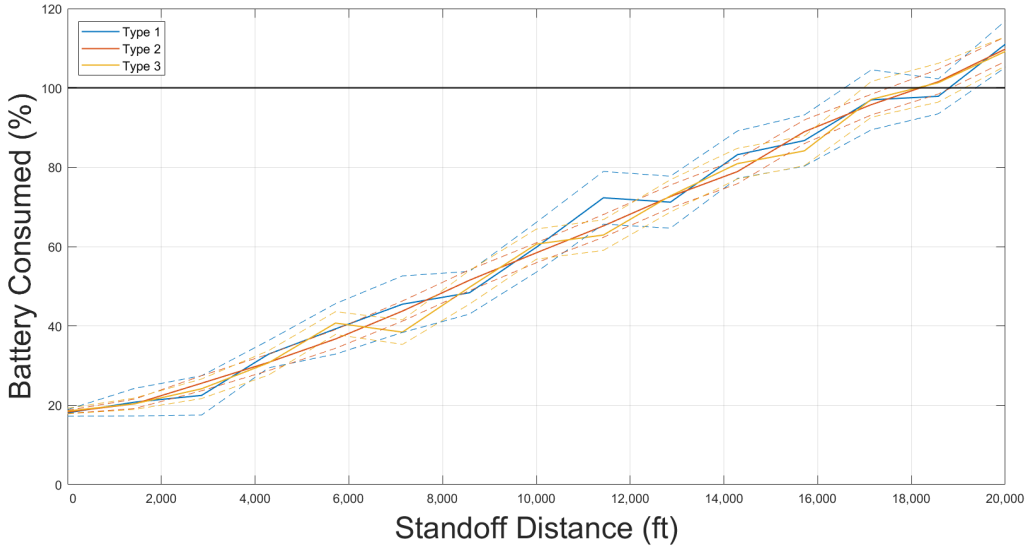

Figure 36: Inverted Descent vs. Wind Fit (95% Confidence)

Figure 37 and Table 17 helped to provide more insight into the weight limitations of the inverted system, governed by its thrust capabilities. Increasing payloads resulted in decreasing potential standoff distance, as expected. While it was recognized that highest payload of 7.2 lbs would certainly not be possible in the current system, it was included in simulation to bracket the Inverted Descent Quadrotor′s performance from no payload, to

maximum theoretical payload. The true performance would lie somewhere between these values depending on payload weight, and will require further testing. At its current state the Inverted Descent Quadrotor could likely be successfully implemented for reconnaissance missions or delivering small sensors/payloads, with strong evidence of potential to scale into larger systems.

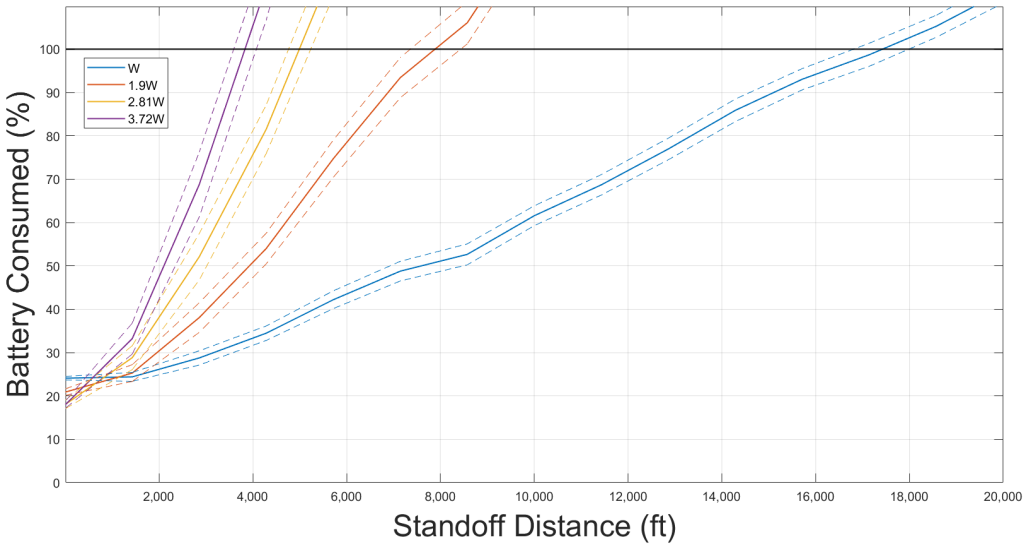

Figure 37: Payload Potential

Table 17: Payload Potential Summary

System Weight	Payload (lbs)	Maximum Standoff Distance (ft)
W	0	17,760
1.9W	2.4	8,269
2.81W	4.8	5,290
3.72W	7.2	3,954

A final comparison, as shown in Table 18, of the Inverted Descent Quadrotor and the predominant PAD methods implemented currently helped to illuminate the promise of the system developed. With translational capabilities on the same order as the parachute/parafoil systems, coupled with much higher precision, flexibility and descent rates, the Inverted Descent Quadrotor proved the potential viability of this novel PAD system.

Table 18: Comparison of PAD Systems

System	Payload (lbs)	Translation Potential	CEP (ft)
Mosquito	3 – 50	3	98
Micro Onyx	0 – 20	4	246
Snowflake ADS	0 – 3	2	82
Inverted Descent Quadrotor	0 – 5	1.75	0*

*Assuming no sensor error

6.3 Conclusions

The simulation environment helped to illuminate the potential of the Inverted Descent Quadrotor, by providing context to the results seen from testing in a mission setting. The simulation verified the issues plaguing conventional quadrotor descent, displayed how the inverted system overcame these issues and gave a good faith prediction of the potential of the Inverted Descent Quadrotor when compared to current PAD methods. While a simulation environment can never exactly reflect real world performance, implementing real wind, experimentally derived data, and Monte Carle methods helped to improve the trust that could be afforded to the simulation used.

In the simulated environment, the Inverted Descent Quadrotor was able to consistently achieve mission distances of $\sim$17,800 ft when released from 10,000 ft regardless of wind prediction quality, and deliver payloads precisely at distances of 5,280 ft even while laden with payloads of 4.8 lbs. With the data available currently, the Inverted Descent Quadrotor showed promise for further implementation into mission level testing and practical use.

CHAPTER 7

CONCLUSIONS AND FUTURE WORK

7.1 Conclusions

In short, with room to still improve in aspects relating to glide and power performance, the Inverted Descent Quadrotor development described was overall successful in developing and vetting a novel method of precision aerial delivery. Performance of inverted descent test flight showed promise for the Inverted Descent Quadrotor as not only a viable alternative to current PAD systems, but as a cutting edge system capable of previously unattainable mission complexity and precision. Implementing quadrotor systems into precision aerial delivery shows promise to change the landscape of the field, and more effectively perform in scenarios requiring the highest level of maneuverability.

Wind tunnel testing achieved the goals of quantifying the potential for inverted descent, and suggesting an optimum baseline throttle for operation. Development of the single axis bi–rotor prototype improved confidence in the feasibility of inverted descent, and yielded further data regarding power, control and glide performance.

The flight performance of the Inverted Descent Quadrotor was successfully characterized through descent testing. While further experiments would help increase confidence in results, the full factorial experiment gave sufficient confidence with which to compare inverted descent to both normal descent as well as move forward with in simulation.

The simulations performed managed to validate the potential of the Inverted Descent Quadrotor as a functional PAD system, with increased accuracy and mission flexibility in low weight, high consequence mission scenarios. Compared to other industry PAD systems, the Inverted Descent Quadrotor proved promising for further development and implementation into PAD.

7.2 Future Work

Logical next steps for this line of research are further testing of the system from greater altitudes, and with increasing payloads to verify simulation results. A likely extension would also be to scale the system used, to gain greater payload capacity.

Attempts have been successful to improve glide capabilities up to as high as 0.4, as seen in Figure 38 in the ″fin design″. The fin modified the drag during descent to act in conjunction with the thrust for translation as seen in Equation 7.1. This allowed for greater glide capability, and eliminated the issue of increased control through increased baseline throttle resulting in less glide capability. The crude prototype implemented consisted of foam board fixed to the underside of the quadrotor, as shown in Figure 39.

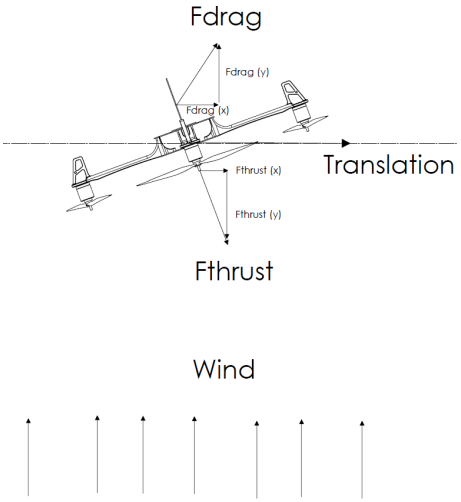

Figure 38: Fin Free Body Diagram

Figure 39: Inverted Descent Quadrotor with Fin

$$\sum F_x = ma_x = F_{drag,x} + F_{thrust,x} \tag{7.1}$$

This design, while effective in descent, greatly reduced normal flight control and required no wind to successfully achieve the ascent for testing. Future designs would likely include a retractable fin to regain normal flight characteristics post descent. Another option to increase glide would be to fashion custom quadrotor arms that serve as airfoils during descent.

Future development seems ripe with opportunity in this novel descent regime, with potential for much innovation. The testing performed seemed to suggest promise for further work regarding the Inverted Descent Quadrotor.

APPENDIX A

INFORMATION

Table 19: Full System Baseline Throttle Experiment Sample Size

Plot	Throttle	Number of Samples
Power	0	1
	10	1
	20	3
	30	8
	40	12
Roll, Pitch, Yaw	0	2
	10	2
	20	2
	30	3
	40	4

Table 20: Full Factorial Descent Experiment

Configuration	Descent Style	Maneuver
1	Slow	0
2	Slow	10
3	Slow	20
4	Slow	30
5	Medium	0
6	Medium	10
7	Medium	20
8	Medium	30
9	Fast	0
10	Fast	10
11	Fast	20
12	Fast	30
13	Inverted	0
14	Inverted	10
15	Inverted	20
16	Inverted	30

Table 21: Descent Testing Sample Size

Descent Style	Maneuver	Power/Energy	Roll/Pitch/Yaw/Glide
Slow	0	1	1
	10	1	1
	20	3	6
	30	1	1
Medium	0	1	3
	10	1	2
	20	2	3
	30	1	1
Fast	0	1	3
	10	1	2
	20	1	4
	30	1	1
Inverted	0	1	1
	10	1	1
	20	1	1
	30	3	3

REFERENCE LIST

[1] Yakimenko, O. A., "Recent advances and new horizons in aerial payload delivery," *2011 9th IEEE International Conference on Control and Automation (ICCA)*, 2011, pp. 148–152. doi:10.1109/ICCA.2011.6137933.

[2] Grau, L. W., and Thomas, T. L., "'Soft Log'and Concrete Canyons: Russian Urban Combat Logistics in Grozny," *Marine Corps Gazette*, Vol. 83, 1999, pp. 67–75.

[3] Talaeizadeh, A., Pishkenari, H. N., and Alasty, A., "Quadcopter Fast Pure Descent Maneuver Avoiding Vortex Ring State Using Yaw-Rate Control Scheme," *IEEE Robotics and Automation Letters*, Vol. 6, No. 2, 2021, pp. 927–934. doi:10.1109/LRA.2021.3052436.

[4] Meier, D. C., "Application of Satellite-Derived Wind Profiles to Joint Precision Airdrop System (JPADS) Operations," *AFIT Theses and Dissertations*, 2010, p. 2171. URL https://scholar.afit.edu/etd/2171.

[5] Tavan, S., "Status and context of high altitude precision aerial delivery systems," *AIAA Guidance, Navigation, and Control Conference and Exhibit*, 2006, p. 6793. doi:10.2514/6.2006-6793.

[6] Benney, R., Barber, J., McGrath, J., McHugh, J., Noetscher, G., and Tavan, S., "The Joint Precision Airdrop System Advanced Concept Technology Demonstration," *18th AIAA Aerodynamic Decelerator Systems Technology Conference and Seminar*, Vol. 1601, AIAA, 2005. doi:10.2514/6.2005-1601.

[7] Yakimenko, O. A., Slegers, N. J., Bourakov, E. A., Hewgley, C. W., Bordetsky, A. B., Jensen, R. P., Robinson, A. B., Malone, J. R., and Heidt, P. E., "Mobile system for precise aero delivery with global reach network capability," *2009 IEEE International Conference on Control and Automation*, 2009, pp. 1394–1398. doi:10.1109/ICCA.2009.5410590.

[8] Cinnamon, A., Miller, E., and Gilkey, A., "Analysis of Performance Metrics for Precision

Airdrop," *24th AIAA Aerodynamic Decelerator Systems Technology Conference*, June 2017. doi:10.2514/6.2017-3225, URL https://arc.aiaa.org/doi/abs/10.2514/6.2017-3225.

[9] Klinkmueller, K., Wieck, A., Holt, J., Valentine, A., Bluman, J. E., Kopeikin, A., and Prosser, E., "Airborne Delivery of Unmanned Aerial Vehicles via Joint Precision Airdrop Systems," *AIAA Scitech 2019 Forum*, 2019. doi:10.2514/6.2019-2285, URL https://arc.aiaa.org/doi/abs/10.2514/6.2019-2285.

[10] Talaeizadeh, A., Antunes, D., Pishkenari, H. N., and Alasty, A., "Optimal-time quadcopter descent trajectories avoiding the vortex ring and autorotation states," *Mechatronics*, Vol. 68, 2020, p. 102362. doi:https://doi.org/10.1016/j.mechatronics.2020.102362, URL https://www.sciencedirect.com/science/article/pii/S0957415820300428.

[11] Tiemann, C. A., "Viability and Validation of Near-Passive Descent Control for Quadrotor Systems," Master's thesis, University of Missouri - Kansas City, 2020. URL https://mospace.umsystem.edu/xmlui/handle/10355/74346.

[12] Rodic, A., and Mester, G., "Control of a quadrotor flight," *Proceedings of the ICIST Conference*, 2013, pp. 61–66.

[13] Sabatino, F., "Quadrotor control: modeling, nonlinearcontrol design, and simulation," Master's thesis, KTM Royal Institute of Technology, Sweden, 2015.

[14] Woolf, P., *Chemical Process Dynamics and Controls*, Open textbook library, University of Michigan Engineering Controls Group, 2009. URL https://books.google.com/books?id=Op87vwEACAAJ.

[15] Del Cont Bernard, D., Giurato, M., Riccardi, F., and Lovera, M., "Ground Effect Analysis for a Quadrotor Platform," *4th CEAS Specialist Conference on Guidance, Navigation & Control*, Springer, 2018, pp. 351–368. doi:10.1007/978-3-319-65283-2_19.

[16] Czyba, R., and Szafranski, G., "Control Structure Impact on the Flying Performance of the Multi-Rotor VTOL Platform - Design, Analysis and Experimental Validation," *International Journal of Advanced Robotic Systems*, Vol. 10, 2013, p. 1. doi:10.5772/53747.

[17] Vandoren, V., "Fundamentals of cascade control," *Control Engineering*, 2021. URL https://www.controleng.com/articles/fundamentals-of-cascade-control/.

[18] Houtz, A. D., and Cooper, D., "Category Archives: Cascade Control For Improved Disturbance Rejection," , Apr 2015. URL https://controlguru.com/category/cascade-control-for-improved-disturbance-rejection/.

[19] Theys, B., and Schutter, J. D., "Forward flight tests of a quadcopter unmanned aerial vehicle with various spherical body diameters," *International Journal of Micro Air Vehicles*, Vol. 12, 2020, p. 1756829320923565. doi:10.1177/1756829320923565, URL https://doi.org/10.1177/1756829320923565.

[20] Haller, J., Fields, T., and Yakimenko, O. A., "Precision Aerial Delivery with a Steerable Cruciform Parachute," *24th AIAA Aerodynamic Decelerator Systems Technology Conference*, 2017, p. 3539. doi:10.2514/6.2017-3539.

[21] Paredes, J. A., Saito, C., Abarca, M., and Cuellar, F., "Study of effects of high-altitude environments on multicopter and fixed-wing UAVs' energy consumption and flight time," *2017 13th IEEE Conference on Automation Science and Engineering (CASE)*, 2017, pp. 1645–1650. doi:10.1109/COASE.2017.8256340.

VITA

Sean Ward was born on April 9, 1997 in St. Louis, Missouri. He attended Rockwood Summit High School in Fenton, MO and graduated in 2015. In 2020, he graduated Magna Cum Laude from the University of Missouri Kansas City with a Bachelor′s of Science Degree in Mechanical Engineering. Since graduation, he has worked as a graduate research assistant under Dr. Travis Fields in the Parachute and Aerial Vehicle Systems laboratory. Sean′s research has focused on the development of an inverted descent method for quadrotors.